DISCOVERY OF MONOCLONAL ANTIBODIES FOR DIAGNOSTICS AND THERAPIES USING CONJUGATE VIRUS-LIKE PARTICLE VACCINES

A Thesis
Presented to
The Academic Faculty of Georgia Institute of Technology

by

Michelle Schroeder

In Partial Fulfillment
of the Requirements for the Research Option
School of Chemistry and Biochemistry, Georgia Institute of Technology

Georgia Institute of Technology, May 2021

DISCOVERY OF MONOCLONAL ANTIBODIES FOR DIAGNOSTICS

AND THERAPIES USING VIRUS-LIKE PARTICLE VACCINES

Approved By

Dr. M.G. Finn
School Chemistry and Biochemistry
Georgia Institute of Technology

Dr. Susan Thomas
George W. Woodruff School of Mechanical Engineering
Georgia Institute of Technology

Georgia Institute of Technology, May 2021

ACKNOWLEDGMENTS

I would like the thank Prof. M.G. Finn for the guidance and opportunities he has provided me throughout the course of this project. I would also like to thank Dr. Asheley Chapman for her constant support and mentorship throughout my undergraduate career. This work was funded in part by the Presidents Undergraduate Research Award from the Georgia Institute of Technology and the Beckman Scholarship from the Arnold and Mabel Beckman Foundation.

LIST OF FIGURES AND TABLES

Chapter 2

Scheme 1. Method of monoclonal antibody development

Chapter 3

Figure 1. Three-dimensional structures of PP7 and Qβ

Table 1. Potency and lethality of common opioids and their derivatives

Chapter 4

Table 1. SARS-CoV-2 peptide immunization schedule

Chapter 5

Figure 1. Structure of fentanyl derivatives for vaccine conjugates

Figure 2. Analysis of fentanyl 13a immunogenicity by adjuvant

Figure 3. Immunogenicity of eight fentanyl derivative VLP conjugate vaccines

Figure 4. Statistics from fentanyl hybridoma fusions

Figure 5. Subclass determination of fentanyl derivative mAbs

Figure 6. Cross reactivity of mAbs to eight fentanyl derivatives

Figure 7. Distinguishing derivatives using mAbs.

Figure 8. Analysis of linker location effect on fentanyl mAbs

Figure 9. Cross reactivity of fentanyl 13a mAbs to naloxone

Figure 10. Structure of SARS-CoV-2 peptides for vaccine conjugation

Figure 11. Immunogenicity of SARS-CoV-2 peptide VLP conjugate vaccines

Figure 12. Statistics from SARS-CoV-2 peptide fusions

Figure 13. Binding preference of SARS-CoV-2 peptide mAbs

Figure 14. Binding affinities of SARS-CoV-2 peptide mAbs

Figure 15. Immunogenicity of SARS-CoV-2 mutant peptide VLP-conjugate vaccines

Figure 16. Binding preference of SARS-CoV-2 mutant peptide mAbs

Figure 17. Structure of α-amanitin and microcystin LR for vaccine conjugates

Figure 18. Immunogenicity of α-amanitin and microcystin LR VLP conjugate vaccines

Figure 19. Statistics from α-amanitin and microcystin LR fusions

Figure 20. Analysis of microcystin LR mAbs' binding preference and affinities

SYMBOLS AND ABBREVIATIONS

Monoclonal Antibodies (mAbs)

Immunoglobulin G (IgG)

Virus-like Particle (VLP)

Centers for Disease Control and Prevention (CDC)

Antibody Binding Site (ABS)

Antigen Presenting Cells (APCs)

B Cell Receptor (BCR)

messenger Ribose Nucleic Acid (mRNA)

Toll-like Receptor (TLR)

Immunoglobulin M (IgM)

Invariant Natural Killer T cell (iNKT)

Median Lethal Dose (LD_{50})

Median Effective Dose (ED_{50})

World Health Organization (WHO)

Angiotensin-Converting Enzyme 2 (ACE2)

Receptor Binding Domain (RBD)

N-terminal Domain (NTD)

β-D-1-Thiogalactopyranoside (IPTG)

Dynamic Light Scattering (DLS)

Fast Protein Liquid Chromatography (FPLC)

Liquid Chromatography-Mass Spectrometry (LCMS)

TABLE OF CONTENTS

ACKNOWLEDGEMENTS……..…..……iii

LIST OF FIGURES AND TABLES..……iv

SYMBOLS AND ABBREVIATIONS……...vi

CHAPTER

1. Abstract……3
2. Introduction.…….……4
3. Literature Review
    - 3.1. MAbs, VLPs, and Hybridoma Technology……..8
    - 3.2. Fentanyl Derivatives.……..12
    - 3.3. SARS-CoV-2 Peptides……15
    - 3.4. α-Amanitin and Microcystin Toxins.……..17
4. Materials and Methods
    - 4.1. Transformation and Particle Expression..……18
    - 4.2. Particle Purification and Characterization...……18
    - 4.3. Particle Modification.……...……...……19
    - 4.4. Immunization and B cell Perfusion...…...……20
    - 4.5. Serum ELISAs…..……...……22
    - 4.6. Hybridoma Development (Conducted at CDC)....….…….……23
    - 4.7. Clonal Selection and Functional Determination.……23
5. Results and Discussion
    - 5.1. Fentanyl Derivatives
        - 5.1.1. Fentanyl Derivative Selection and Structures……..25

5.1.2. Immunization Strategy Optimization……...27

5.1.3. All Derivative Immunizations……..31

5.1.4. Hybridoma Fusion and Clone Characterization……33

5.1.5. MAb Functionality……...35

5.1.6. Conclusions and Future Experimentation……40

5.2. SARS-CoV-2 Peptides

5.2.1. Peptide Selection and Structures……..42

5.2.2. Peptide Immunizations……43

5.2.3. Hybridoma Fusion and Clone Characterization……45

5.2.4. Mutant Peptide……49

5.2.5. Conclusions and Future Experimentation……53

5.3. Amanitin and Microcystin Toxins

5.3.1. Toxin Structures……...54

5.3.2. Toxin Immunizations……...55

5.3.3. Hybridoma Fusion and Clone Characterization……...56

5.3.4. Conclusions and Future Experimentation……58

6. Conclusions……...……60

REFRENCES……62

APPENDIX A……67

APPENDIX B……74

ABSTRACT

Monoclonal antibodies (mAbs) are highly specific antigen binding proteins that are used as biological reagents, therapeutics, and in rapid diagnostics. While mAbs have extensive potential applications, their means production for small molecules and conformationally specific peptides is difficult. Here, we use a method of mAb production in which we pair conjugate virus-like particle (VLP) vaccine with hybridoma technology to produce high-affinity mAbs against three classes of molecules 1) fentanyl derivatives, 2) SARS-CoV-2 peptides, and 3) α-amanitin and microcystin cyclic peptide toxins. We successfully produced broad and derivative-selective mAbs against eight fentanyl derivatives. We also showed early signs of success targeting neutralizing and mutant SARS-CoV-2 peptides with conformational specificity using a heterologous prime-boost strategy. Lastly, we produced high affinity mAbs for both α-amanitin and microcystin, two highly toxic cyclic peptides. The early success of mAb production against the variety of targets presented in this thesis shows the viability and exceptional versatility of conjugate VLP vaccines as a means to producing mAbs.

INTRODUCTION

Monoclonal antibodies (mAbs) are immune cell derived proteins that have been at the forefront of biomedical research over the past 40 years. Their unique characteristics give them the potential to create cheap, fast, and accurate diagnostics as well as novel therapeutics. MAbs are identical immunoglobulins derived from the same clonal cell line that bind a unique epitope. They have shown tremendous promise as both diagnostics and clinical therapies due to their high specificity, strong antigen binding affinity, and relatively low cost to synthesize in large quantities.[1, 2] Currently, their uses range from home pregnancy and drug tests to the clinical diagnosis and treatment of a variety of cancers, infectious diseases and autoimmune disorders.[3, 4]

While mAbs hold the potential to bind a huge variety of antigens, allowing them countless potential applications, the biosynthetic process of mAb development poses limitations on acceptable antigen targets. This process relies on the ability of animal immune systems to produce high affinity immunoglobulin G (IgG) against the antigen of interest. Some antigens (including certain viral proteins) are naturally very immunogenic helping this immune response to occur, however others such as small molecule haptens and carbohydrates lack this ability. There are multiple immunological processes that help initiate this strong humoral response including uptake and presentation of the antigen by antigen presenting cells (APCs), engagement of the compliment cascade, proinflammatory $CD4^+$ T cell response, and effective B cell receptor (BCR) crosslinking.[5] One way to overcome the limitations of some antigens is by use of a conjugate vaccine platform such as virus-like particles (VLPs), which are capable of activating these immunological processes.

VLPs are immunogenic protein nanoparticles derived from bacteriophage that can be genetically engineered or covalently modified to present an antigen of interest. VLPs of great

interest to our work, VLP Qβ and PP7, originate from *Leviveridiae* bacteriophage. They have multiple characteristics that allow them to engage each previously stated immunological process needed to activate humoral immunity. First, they are able to activate APCs through packaged mRNA, a ligand for TLR7 and TLR8 that when bound initiate antigen presentation and proinflammatory cytokine responses.[5, 6] Since VLPs are proteins, they are also capable of major histocompatibility complex (MHC) class II presentation, which is necessary for B cell activation and affinity maturation.[7] Their highly repetitive structure is also necessary for BCR cross linking which engages the classical pathway of the compliment cascade and facilitates B cell activation.[5] Lastly, Qβ and PP7 are roughly 28 nm in diameter which allows them to drain into the lymph nodes, increasing B cell exposure to antigens[8] and resulting in IgG production and affinity maturation. VLPs are able to confer this immunogenicity to molecules covalently attached to them. We hypothesize based on the high-quality antibodies that result from conjugate VLP vaccines that this platform could be an ideal method of initial animal immunization with the ultimate goal of mAb discovery.

In addition to helping establish a proof of concept for the viability of VLP vaccines in the development of mAbs, each target molecule presented in this thesis, diverse in structural classification, poses a public health risk that the production of mAbs stands to help alleviate. Small molecule fentanyl and its derivatives are synthetic opioids that have been the leading cause of overdose deaths in the United States since 2015.[9] Some of these derivatives still lack proper diagnostics tools, underscoring a need for the diagnostic mAb development and, if humanized, could serve as a passive biological therapy for overdose victims. SARS-CoV-2, the viral agent responsible for the COVID-19 pandemic, has resulted in millions of deaths worldwide.[10] There is a dire need for the creation of mAbs against SARS-CoV-2 viral peptides that could be used for

fast and inexpensive diagnosis. Finally, cyclic peptide microcystin-LR and α-amanitin are natural products found in freshwater cyanobacteria and some species of mushrooms, respectively. Both are toxic to humans and animals and have a high risk for contamination of drinking and agricultural water supplies, creating a need for the development of a fast-acting field diagnostic to test for the presence of these toxins.[11, 12] While each of these targets differ considerably from one another, they all pose a significant threat to human health that can be at least partially alleviated via mAb applications.

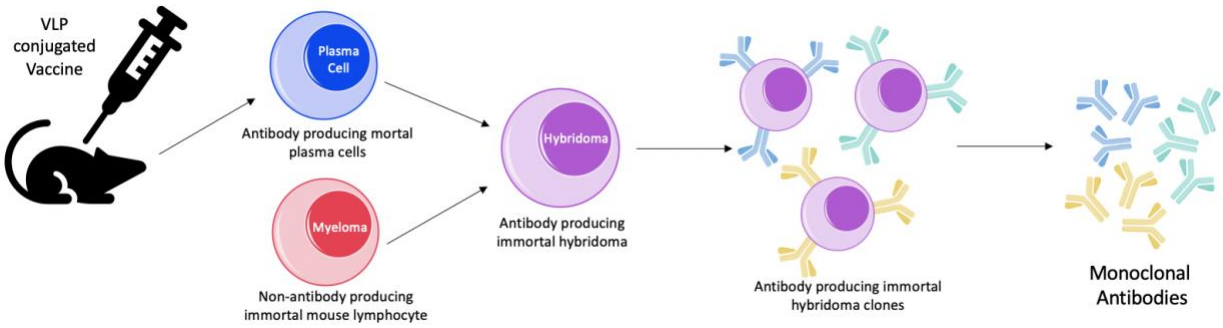

Scheme 1. Method of production of monoclonal antibody producing hybridoma clones from vaccinated mouse plasma cells.

In this project, we overcome the limitations presented by certain target molecules by pairing conjugate VLP vaccine platforms with hybridoma technology in order to discover mAbs against designer drug haptens, viral peptides, and toxins (Scheme 1). Chemically ligated PP7 and Qβ conjugate VLP vaccines were generated against a panel of fentanyl derivatives, several SARS-CoV-2 spike protein peptides, and the toxins microcystin-LR and α-amanitin. Additionally, we genetically engineered PP7 VLPs to display several more SARS-CoV-2 spike protein peptides. We immunized mice with each of these vaccines, as well as conducted various combination immunizations between the SARS-CoV-2 peptide VLPs and the unconjugated whole protein. Once high affinity IgG producing B cells were derived, hybridoma technology was used to electrofuse solenocyte B cells with immortal myeloma derived from murine lymphocytes by our

collaborators at Centers for Disease Control and Prevention (CDC, Scheme 1). The resultant hybridomas created clonal lines capable of producing a large supply of mAbs. Each clone was screened for antigen specificity and multiple positive clones were discovered for each target. Biophysical characterization of antigen specific clones was determined describing binding affinity, and IgG isotype. Antibody function was further explored by determining selectivity, cross reactivity of fentanyl and toxin mAbs to similar antigens and neutralization ability of SARS-CoV-2 mAbs. The success of mAb production against our array of antigenic targets as well as the various immunization strategies presented in this thesis, shows the viability and exceptional versatility of conjugate VLP vaccines as a means to ultimately producing mAbs.

LITERATURE REVIEW

Monoclonal Antibodies, Virus-like Particles, and Hybridoma Technology

Monoclonal Antibodies (mAbs) are identical immunoglobulins that are produced from clonal plasma cells which share a unique parent B cell. Kohler and Milstein were awarded the Nobel prize in 1984 for their development of a method to biosynthesize mAbs.[13] Since this discovery, mAbs have shown tremendous promise as both diagnostics and therapeutics due to their high specificity, strong antigen binding affinity and relatively low cost to synthesize in large quantities.[1, 2] Their value was first seen in bioassay applications, where they are now commonly used as reagents.[14] The development of mAb humanization methods unlocked their potential in a clinical setting. The first FDA approved mAb for clinical use was designed for the prevention of kidney transplant rejection.[15] Now, there are over 100 approved mAbs for use as therapies against cancers, infectious diseases, auto immune diseases and more.[16] Monoclonal antibody therapeutics are also extremely profitable; their annual sales are expected to reach over $130 billion by 2023.[17]

The utility of mAbs comes from their ability to bind an epitope, the region on the antigen recognized by the antibody, with a very high specificity and affinity. The development of novel mAbs first requires the synthesis of a vaccine for the antigen of interest followed by animal immunization, plasma cell extraction via splenectomy and finally, plasma cell fusion with myeloma to create immortal cell lines selected based on its ability to bind the immunogen.[18] While this is initially a labor intensive process, once the clonal cell line for an mAb is produced, its mass production is relatively simple and cost effective.[18]

The first difficulty that arises in the discovery of mAbs is the development of a vaccine for the antigen of interest. Despite the ability of antibodies to bind a vast array of epitopes, initiating the correct immune response that leads to antibody production in mouse models can prove

challenging. While many antigens, including multivalent viral and bacterial proteins, are naturally very immunogenic, others such as small molecules and carbohydrates lack the ability to activate the critical components of humoral immunity necessary for high affinity immunoglobulin G (IgG) production.[6] One way to overcome the limitations of some antigens is by use of a conjugate vaccine platform such as virus-like particles (VLPs), which are capable of activating these immunological processes.

Virus-like particles are non-infectious protein nanoparticles that mimic viral structures and can be genetically engineered or covalently modified to present an antigen of interest.[19] Chimeric VLPs are a type of VLP that use a self-assembling recombinant viral envelope protein linked to a display molecule thus allowing a limitless versatility of antigens capable of being presented by a VLP. Chimeric VLPs have multiple characteristics that make them an ideal vaccine platform for antibody production (Figure 1). Since VLPs are proteins, they are capable of binding major histocompatibility complex (MHC) class II unlike non-protein antigens.[7] This is a vital component of antigen presentation that allows for $CD4^+$ T cell activation, thereby promoting B cell activation and affinity maturation through IL-6 and IL-21 cytokine interactions.[6, 20] VLPs also spontaneously self-assemble in induced *E. coli* cells which allows them to package free floating mRNA.[5] This mRNA is a ligand for Toll-like receptor (TLR) 7 and TLR8 which help engage the APCs necessary for T cell priming and B cell activation.[6] The size and shape of VLPs also plays a significant role in their immunogenicity. VLPs PP7 and Qβ are typically ~28nm in diameter, allowing them to drain into lymph nodes independently of cellular transport which has been shown to increase antigen exposure to B cells.[8] VLPs also have highly repetitive structures. This helps activate B cells both directly through cross linking of BCRs, especially immunoglobulin M (IgM), and indirectly through engagement with the classical pathway of the compliment cascade which also

facilitates B cell activation.[5] The variety of mechanisms by which VLPs interact with humoral immunity allows them to both elicit IgG production and promote affinity maturation. We hypothesize that the high-affinity antibodies that result from conjugate VLP vaccines will make them an ideal method of animal immunization with the goal of mAb discovery.

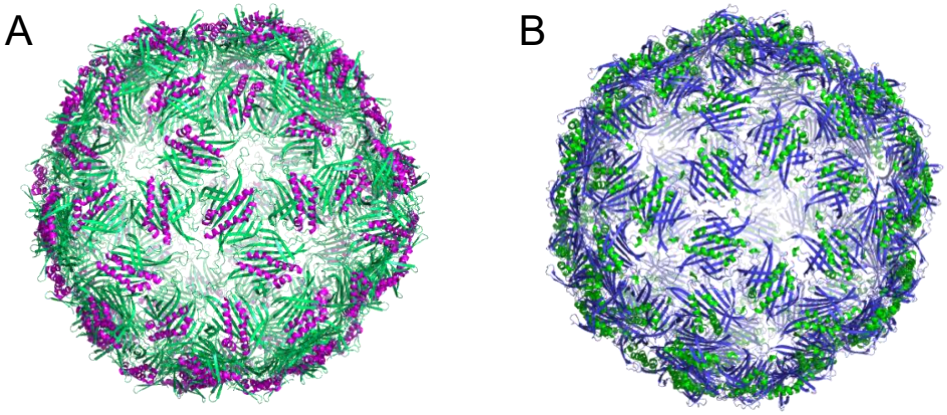

Figure 1. Cryo-EM structure of PP7 [PDB ID: 1DWN] (A) and Qβ [PDB ID:1QBE] (B) VLPs.

Two commonly used VLP platforms are Qβ and PP7 (Figure 2). They are both icosahedral, nonenveloped VLPs that are recombinantly derived from single-stranded RNA bacteriophages.[21, 22] Both VLP capsids are assembled from 180 repeating coat protein units that are stabilized through noncovalent interactions as well as inter-subunit disulfide bonds.[23-25] These strong noncovalent and covalent interactions allow Qβ and PP7 to be chemically modified under a variety of conditions without losing the integrity of the protein structure. Each coat protein has seven lysine residues and a terminal amine that serve as nucleophiles in bioconjugation reactions involving N-hydroxysuccinimide (NHS) and subsequent chemical modification, making them great candidates for multivalent small molecule and carbohydrate antigen presentation. Additionally, both VLPs, when subject to genetic modification, have been shown to successfully to display short surface peptides at either the C- or N-terminus.[26, 27] Both Qβ and PP7 provide exceptional VLP vaccine platforms due to their versatile antigen presentation abilities.

Once a vaccine against the antigen of interest has been successfully made, an effective immunization schedule and adjuvant must be chosen to help bolster murine immune responses. Adjuvants are substances that can be added to a vaccine to increase overall effectiveness while decreasing the number of doses required to obtain a desired immune response.[28] Adjuvants are able to accomplish this in a variety of ways. Freud's Adjuvants and TiterMax® Gold (TMX) does this by the creation of an oil in water emulsion which creates both an antigen depot and the site of injection and causes retention of the antigen in the lymphoid tissue.[29, 30] As discussed previously, localization in the lymph nodes is a vital to antigen exposure to B cells. Another mechanism that some adjuvants utilize is the activation of innate immune cells that increase B cell activity through costimulatory molecules. α-galactosylceramide is an invariant natural killer T cell (iNKT) agonist that accomplishes this by binding CD1d receptor on iNKT cells.[31, 32] These cells in turn produce large amounts of INF-γ, a cytokine that helps stimulate adaptive immune responses.[6] Both TMX and NKT agonist adjuvants have been shown to encourage antibody immune responses and therefore are ideal candidates to be used during vaccination for our method of mAb discovery.

Inducing mouse immune systems to generate high affinity antibodies against the antigen of interest is only half the battle. Once achieved, the B cells that make those antibodies must be extracted and fused with myeloma (immortal mouse lymphocytes) in order to create a hybridoma which can make an immortal line of IgG-secreting clones.[18] Once the hybridoma are generated, each cell must be separated, and its secreted antibodies tested for antigen specific IgG production.[18] To do this our collaborators at CDC use a high throughput hybridoma screening method in which the cells are suspended in a semi-solid media containing a colorimetric substrate that identifies IgG secretion.[33] Automated selection of the positive colonies is performed using a ClonePix instrument. This allows for hundreds of positive clone lines to be picked from a single fusion.

Conjugate VLP immunization paired with hybridoma technology was used to create high affinity mAbs against three distinct sets of molecules. Fentanyl and its derivatives are small molecules that are not naturally immunogenic; by conjugating them with a VLP we were able to produce strong humoral immune responses. While the SARS-CoV-2 spike protein *is* highly immunogenic, by conjugating spike protein peptides to VLPs we were able to generate an immune response against those specific peptides, allowing us to generate antibodies against known neutralizing epitopes as well as high-profile mutant epitopes. Microcystin-LR and α-amanitin are cyclic peptides that have a high toxicity; by conjugating them with a VLP we are able to increase their immunogenicity while decreasing toxicity. Each of these groups of molecules also pose a threat to human health that high affinity mAbs have the potential to help alleviate.

Fentanyl Derivatives

Fentanyl is a synthetic opioid derivative used clinically as an anesthesia and as an analgesic to treat post-operative, acute or terminal pain. After first being synthesized in 1960, it was hailed by clinicians for its high potency, allowing it to adequately treat pain in very small doses.[34] In fact, to this day fentanyl and its derivatives are some of the most active known mu-opioid receptor agonists.[35] Fentanyl has a nearly 1000x higher potency than morphine and its analogue carfentanil has a nearly 10,000x higher potency (Table 1). This high potency, while clinically valuable, has made fentanyl popular target for illicit drug use.

Fentanyl is responsible for a rapidly increasing number of overdose deaths each year. Fentanyl and its derivatives have become the leading cause of overdose deaths in the United States resulting in 60,000-80,000 deaths each year since 2016.[9, 36] This increase can be attributed to both its increasing popularity due to an over 30x higher potency than heroin and the risk associated with

taking it as it is over 7x more lethal than heroin (Table 1). In addition to intentional fentanyl use, it has also emerged on the black market as a filler in other illicit narcotics like heroin and cocaine.[37] Unintentional fentanyl consumption by individuals taking other drugs is responsible for over half of overdose deaths today.[38, 39]

Table 1. Relative opioid potencies and lethalities. All measurements taken in Sprague-Dawley rats after intravenous administration and determined by similar methods.

Opioid	ED_{50} (mg/kg)	LD_{50} (mg/kg)	Relative Potency	Relative Lethality
Morphine	3.21[40]	223[40]	1	1
Heroin	0.129[41]	22.5[42]	25	10
Fentanyl	0.0039[43]	3.05[35]	823	73
Carfentanil	0.0004[44]	3.39[35]	8025	67

Monoclonal antibodies have the potential to help curb the current fentanyl epidemic in a variety of ways. First, we hypothesize they can be used in immunoassay diagnostics to rapidly, reliably, and inexpensively detect and distinguish fentanyl and its analogues in circulation from other opioids. These diagnostics could help medical professionals better treat overdose victims and trace its origins. The elimination half-life of fentanyl in the blood stream is 90-360 minutes which is significantly longer than that of other common narcotics such as heroin which has a half-life of only 9-22 minutes.[45, 46] The elimination half-life of naloxone, the most commonly used overdose reversal medication, is only 30-120 minutes, making repeat fentanyl overdoses after initial treatment a substantial concern.[47] As a result, knowing fentanyl was involved in an overdose significantly impacts the administration schedule of reversal medication. Since compliance in overdose situations can be very low and other drugs are often laced with fentanyl without the user's knowledge, diagnostics that can quickly test for low concentrations of fentanyl in blood or urine are imperative to improving outcomes.

In addition to use in diagnostics, fentanyl binding mAbs have also shown promise as a biological therapy to treat overdose victims. A recent study by Smith, et al. (2019)[48] found that mAbs developed against fentanyl and carfentanil decreased symptoms in mice associated with fentanyl intoxication as well as increased the LD_{50} – the median lethal dose. The elimination half-life of these mAbs in the blood was also shown to be several days, significantly longer than that of fentanyl and naloxone.[48] The mechanism by which mAbs and naloxone can combat opioid intoxication also differ greatly. Naloxone competitively binds opioid receptors, while mAbs neutralize and opsonize fentanyl thereby preventing it from binding the receptors and labeling it for degradation in the blood stream. As a result, it is possible that these two treatments could be combined, with naloxone being used as the fast-acting component and mAbs providing long lasting protection against repeat overdoses.

Toxicity and lack of immunogenicity of these fentanyl derivatives makes producing potentially lifesaving mAbs difficult. In this study, we overcame these limitations by conjugating eight different fentanyl immunogens with alkyne linkers to PP7 VLPs using the Copper catalyzed azide alkyne cycloaddition (CuAAC) reaction. This strategy uses the VLP to engage humoral immunity while creating specificity towards the fentanyl derivatives. The vaccines were then immunized into BALB/c mice until optimal IgG production was elicited (usually 7-9 weeks post prime). Hybridoma were then created through electrofusion of the resultant B cells with murine myeloma. The mAbs derived from the hybridomas were then screened for cognate antigen specificity, cross reactivity with the other derivatives for diagnostic purposes, and cross reactivity to naloxone for therapeutic purposes. Ultimately, we produced 14 mAbs with unique binding patterns to the eight derivatives. These mAbs have the ability to address weaknesses in current diagnostics and therapeutics.

SARS-CoV-2 Peptides

SARS-CoV-2 is an enveloped RNA virus that causes mild to severe respiratory infections, a disease known as COVID-19.[49] As of April 2021 COVID-19 is attributed to nearly 3 million deaths worldwide and over 500,000 in the united states alone.[10] The World Health Organization (WHO) declared COVID-19 a global pandemic in March 2020.[50] Since then, restrictions used to slow the spread of the virus have also crippled world economies and left millions out of work. There has been an urgent need for quality reagents, diagnostics, and therapeutics all of which can be obtained through mAb production. Specifically, there is a need for mAbs that bind known neutralizing epitopes and epitopes containing new emerging mutations.

The SARS-CoV-2 virus contains an ectodomain known as the spike protein. The spike protein is an important element of SARS-CoV-2 pathology as it is responsible for binding angiotensin-converting enzyme 2 (ACE2) which allows it to gain entry into human epithelial cells.[51] The receptor binding domain (RBD) is the portion of the spike protein that makes physical connections to the ACE2 receptor.[52] As a result, this is an important region to target for the creation of neutralizing antibodies. In fact, a large percentage of neutralizing mAbs isolated from infected humans bind the RBD.[53-55] A few have also been isolated that bind to the N-terminal domain (NTD) of the spike protein.[55, 56] Based on these findings, it is clear that certain epitopes on the spike protein are very important to neutralizing antibody development.

In order to target these known neutralizing epitopes, we created a heterologous prime-boost strategy in which we primed with PP7 conjugated to the linear peptide in order to create a targeted immune response. We then boosted with whole protein RBD to ensure the affinity matured antibodies bound the peptide in its native conformational state. To create the VLP-peptide vaccines we used two different conjugation techniques. In one strategy the PP7 plasmid was modified with

the peptide nucleic acid sequence at the C-terminus. In the second strategy, the assembled PP7 particles were conjugated with the peptides modified with an alkyne linker using the CuAAC reaction. We tried both the VLP-peptide immunizations individually and with cocktails containing different VLP-peptide conjugates. The cocktail strategy allows for targeting of multiple epitopes in a single vaccination. The preliminary results are promising that we were able to direct the polyclonal immune response towards our peptides of interest.

In addition to targeting known neutralizing epitopes we also targeted peptides containing important mutations. The Y453F mutation is a high profile mutation in the RBD known to allow transmission between minks and humans.[57] Y453 is an important amino acid since it directly interacts with the ACE2 receptor helping viral entry into cells.[51, 58] The effect of this mutation on binding of previously effective neutralizing mAbs has been tested. These studies have shown that this mutation decreases the neutralizing ability of multiple of these mAbs.[59-61] In this study, we attempt to make mAbs that differentially bind either to Y453F mutant or the wild type. To do this we tried two different heterologous prime-boost strategies based on competing hypotheses. In the first, we primed with VLP-peptide to try to direct the initial immune response towards the peptide, then boosted with RBD to ensure affinity maturation occurs to the peptide in its native conformational state. In the second we primed with RBD to select for germline B cells that bind the RBD then boost with peptide to mature only the fraction that bind the peptide of interest.

To test for peptide and confirmational specificity we used two types of ELISAs. With the first the whole RBD protein was plated to test for conformational specificity; however, this strategy does not confirm binding to the peptide of interest. In the second strategy biotinylated peptide was plated on streptavidin plates to test for peptide specific response. Though this strategy ensures only peptide specific antibodies bind, it could also include antibodies that only bind the linear peptide

and missing ones that need conformational specificity. We found that the RBD prime with peptide boost did a better job at directing the long-term immune response towards the peptide. Ultimately, we were able to isolate mAbs with both wild type and mutant RBD preference.

α-Amanitin and Microcystin toxins

α-Amanitin and microcystin LR are both hepatotoxins that are naturally produced by environmental agents. α-Amanitin is produced by several species of mushroom (including the death cap mushroom), and microcystin is synthesized by fresh water cyanobacteria.[11,12] When ingested, α-Amanitin inhibits RNA polymerase II, resulting in inefficient protein synthesis, cell necrosis, and ultimately liver and kidney failure.[62] Microcystin LR similarly causes liver damage and death, however its mechanism of action involves induced apoptosis from oxidative stress placed on the cell due to interactions between microcystin and protein phosphatases.[63] Both of these toxins have the potential to contaminate water supplies that provide irrigation to crops in large scale farming and clean drinking water for high density populations. The development of a fast-acting field diagnostic to test for the presence of these toxins is crucial to ensure that supplies of water have not been naturally or artificially polluted with these toxins.

The high toxicity and lack of immunogenicity of these cyclic peptides makes producing mAbs for them difficult. In this study, we conjugated each toxin to the Qβ VLP using the CuAAC reaction. We used this conjugate vaccine platform to direct the humoral immune response in BALB/c mice. Once optimal antigen specific IgG titers were obtained the resultant B cells were used to create hybridoma using hybridoma technology. Using this method, we produced dozens of high affinity antigen specific clones for both α-amanitin and microcystin LR. These mAbs will be used in fast acting field diagnostics to test for water contamination with each of these toxins.

MATERIALS AND METHODS

4.1 Transformation and Particle Expression

To produce VLPs, BL21(DE3) chemically competent *Escherichia coli* cells were transformed using heat shock with either PP7 or Qβ bacteriophage derived coat protein pET plasmids containing a kanamycin resistance gene. The transformed cells were plated on positive-selection kanamycin containing agar to prevent non-transformed cell growth and incubated overnight at 37ºC. Single colonies chosen from the plates were added to 125 mL SOB broth starter cultures with kanamycin and incubated overnight at 37ºC with shaking. Thirteen mL of starter culture broth was then added to each 1 L expression culture of kanamycin-containing SOB broth and incubated at 37ºC with shaking until reaching an optical density of 0.9 (usually ~4 h). The cultures were then induced with β-D-1-thiogalactopyranoside (IPTG) and incubated overnight at room temperature with shaking to activate the lac operon controlling nanoparticle transcript. The cultures were pelleted by centrifugation the following day.

4.2 Particle Purification and Characterization

To purify the recombinant particles from the *E. coli* cells, the pellets were each dissolved in 0.1 M KPO_4 buffer (pH 7.4) and lysed by sonication. The lysate was centrifuged, and the pellet containing insoluble cellular components removed. Excess ammonium sulfate was added overnight at 4 ºC to the lysate to precipitate the proteins and centrifuged the following day to form a pellet. The pellet was then resuspended in 0.1 M KPO_4 and the proteins separated from any remaining lipids by organic extraction using an equal volume of 1:1 chloroform: butanol. The recombinantly produced nanoparticles were then purified from other cell proteins using a sucrose gradient (10% to 40%). The blue particle bands were collected by visualization on a gradient fractionator. The particles

were then pelleted by ultracentrifugation and resuspended in 0.1 M KPO_4. Purified particle concentration was determined by Bradford analysis using bovine serum albumin (BSA) standards and Coomassie brilliant blue. Particles were characterized using dynamic light scattering (DLS), fast protein liquid chromatography (FPLC) and liquid chromatography-mass spectrometry (LCMS) to determine particle diameter and monodispersity, purity, and molecular weight, respectively.

4.3 Particle Modification

Particle Modification by Chemical Ligation (Conducted by Asheley Chapman & Robert Hincapie)

Chemically ligated particle modifications were conducted by Asheley Chapman and Robert Hincapie in the lab of Prof. M.G. Finn at Georgia Tech. PP7 particles were modified to display the fentanyl derivatives and RDM, FP and Y453F mutant SARS-CoV-2 peptides; the Qβ particles were modified to display the toxins. The VLPs were modified to display azides using NHS-ester azido-acetate linkers. Alkyne-labeled fentanyl derivatives, SARS-CoV-2 peptides and toxins were installed by copper catalyzed azide alkyne cycloaddition (CuAAC). Conjugates were purified by column chromatography and concentrated by centrifugation. Protein concentrations were determined by Bradford assay and characterization was confirmed by DLS, FPLC and LCMS (Appendix A,B,C).

Particle Modification by Genetic Engineering (Conducted by Liangjun Zhao & Parisa Keshavarz-Joud)

Genetic particle modifications were conducted by Liangjun Zhao and Parisa Keshavarz-Joud in the lab of Prof. M.G. Finn at Georgia Tech. The 6, 9, 16, and 17 SARS-CoV-2 peptide RNA

sequences were cloned into the PP7 plasmids. This allowed for C-terminus display of the linear peptides on each coat protein monomer resulting in multivalent peptide presentation on the assembled nanoparticle. Protein concentrations were determined by Bradford assay and characterization was confirmed by DLS, FPLC and LCMS (Appendix B).

4.4 Immunization and B Cell Perfusion

All animal studies were performed in compliance with the Georgia Institute of Technology Institutional Animal Care and Use Committee and all protocols followed National Institute of Health Guide for the Care and Use of Laboratory Animals Guidelines.

Fentanyl Conjugate Vaccine Immunizations

Six-week-old female BALB/c mice received initial bilateral subcutaneous immunizations on day 0 and subsequent boosts on days 14 and 28. Each mouse received 100 µL total for each immunization containing 50 µg of conjugate vaccine in 0.1 M sterile KPO_4 along with 500 ng of PBS-57 in 1 µL DMSO co-mixed immediately before injection. Mice selected for use in hybridoma development based on serum ELISA screening were given an additional boost with 100 µL of 10 µg conjugate vaccine 3 days prior to harvesting spleens. The mice were bled by submandibular puncture at days 0, 14, 21, 28, 35, and when terminated (varies by vaccine due to scheduling conflicts). Mice selected for harvest were sacrificed using CO_2 on day 35 (CF1, OMe`-Fen), 43 (Fentanyl, NCF1, Acetyl Me-Fen, 3Me-Fen), or 53 (Fen13 and NCF2). Splenectomies were then performed and the B cells from the harvested spleens perfused using 20 mL of Iscove's Modified Dulbecco's Medium (IMDM).

SARS-CoV-2 Peptide Conjugate Vaccine Immunizations

Six-week-old female BALB/c mice received initial bilateral subcutaneous immunizations of the VLP-peptide on day 0 and subsequent boosts of whole protein according to Table 1. Protein amounts per immunization are depicted in Table 1 according to initial conjugate vaccine administered with a total volume of 100 µL in 0.1 M sterile KPO_4 for each. Mice were bled on day 0, 32 (28 for each cocktail) and when terminated. Mice selected for harvest were sacrificed using CO_2. Splenectomies were then performed and the B cells from the harvested spleens perfused using 20 mL of Iscove's Modified Dulbecco's Medium (IMDM) for hybridoma production by CDC.

Table 1. SARS-CoV-2 immunization schedule.

	Primary	Boost 1	Boost 2	Boost 3	Fusion
PP7-covid-6	PP7-covid-6 + NKT 50µg (day 0)	His-S1 +TMX 10µg (day 14)	His-S1 (F1), PP7-covid-6 (F2) 15µg (day 21)	His-S1 +NKT 15µg (day 27)	(day 30)
PP7-covid-16	PP7-covid-16 + NKT 50µg (day 0)	His-S1 +TMX 10µg (day 14)	His-S1 (F1), PP7-covid-6 (F2) 15µg (day 21)	His-S1 + NKT 15µg (day 27)	(day 30)
Cocktail 1	Cocktail 1 (9, 16, 17) 100µg (day 0)	His-S1 + TMX 10µg (day 16)	mFcRBD 10µg (day 27)	His-S1 10µg (day 50)	(day 58)
Cocktail 2	Cocktail 2 (6, 9) 100µg (day 0)	His-S1 + TMX 10µg (day 16)	mFcRBD 10µg (day 27)	mFcRBD 10µg (day 50)	(day 58)
PP7-covid-6-rep	PP7-covid-6 + NKT 75µg (day 0)	mFcRBD 10µg (day 22)	mFcRBD 10µg (day 35)	mFcRBD 10µg (day 48)	(day 51)
PP7-RBM	PP7-FP + NKT 70µg (day 0)	mFcRBD 10µg (day 22)	mFcRBD 10µg (day 35)	mFcRBD 10µg (day 48)	(day 51)
PP7-FP	PP7-FP 100µg (day 0)	Ecto 10µg (day 14)	Ecto 10µg (day 35)	Ecto 10µg (day 49)	(day 52)
PP7-covid-5	PP7-covid-5 50µg (day 0)	mFcRBD 10µg (day 14)	mFcRBD 10µg (day 28)	mFcRBD 10µg (day 49)	(day 52)
PP7-covid-3	PP7-covid-3 70µg (day 0)	mFcRBD 10µg (day 14)	mFcRBD 10µg (day 28)	mFcRBD 10µg (day 42)	(day 45)

Amanitin and Microcystin Conjugate Vaccine Immunizations

Six-week-old female BALB/c mice received initial bilateral subcutaneous immunizations of the VLP-peptide on day 0 and subsequent boosts on days 14, and 35. Each mouse received a 100 µL dose with 30 µg of conjugate VLP vaccine in 0.01 M KPO_4 with no adjuvant. Mice selected for termination based on high ELISA serum titers were given an additional boost with 7 µL of

conjugate VLP vaccine in 0.01 M KPO_4 with 500 ng of PBS-57 adjuvant mixed immediately before injection 3 days prior to splenectomy. The mice were bled on days 0, 7, 14, 21, 35, 42, 49, and 56 by submandibular bleed. Mice selected for harvest were sacrificed using CO_2 on day 56. Splenectomies were then performed and the B cells from the harvested spleens perfused using 20 mL of Iscove's Modified Dulbecco's Medium (IMDM).

4.5 Serum ELISA

Streptavidin ELISAs

Serum antigen specific antibody binding was measured by streptavidin ELISAs. 1 µg/mL streptavidin in 0.1 M PBS was plated overnight at 4°C on high binding ELISA plates. The plates were then washed with 0.1 M PBS with 0.05% tween (PBST). One hundred µL of block casein was plated for 1 hour at room temperature with light shaking to prevent non-specific binding. The plates were subsequently washed with 125 µL PBST three times. Cognate biotinylated antigen was then plated at a concentration of 0.25 µg/mL in blocking buffer for 1 hour at room temperature with shaking. The plates were then washed again with PBST. To generate serum titers, 6 4x dilutions of each serum were plated in duplicate for 1 hour at room temperature then washed again. Secondary antibody goat anti-mouse total IgG HRP (1:2500 dilution) in blocking buffer was plated for 1 hour at room temperature. For the IgM and subclass ELISAs, anti-IgM, IgG1, IgG2a, IgG2b, or IgG3 HRP conjugates were plated instead of the total IgG HRP. The plates were once again washed. The plates were developed for 30 seconds using TMB and quenched using 2N H_2SO_4. The absorbance at 450 nm was measured by plate reader. Serum titers were generated using sigmoidal regression analysis on GraphPad Prism v. 9 of Log10 serum dilution versus absorbance.

Protein ELISAs

Serum antibody specificity to the VLP carrier, or antigen specificity to COVID peptides or Ecto whole proteins, were measured by protein ELISA. We plated 0.25 µg/mL protein in 0.1 M PBS overnight at 4ºC on high binding ELISA plates. The plates were then washed with 0.1 M PBS with 0.05% tween (PBST). One hundred µL of block casein was plated for 1 hour at room temperature with gentle shaking to prevent non-specific binding. The plates were subsequently washed with PBST. To generate serum titers, 6 4x dilutions of each serum were plated in duplicate for 1 hour at room temperature then washed again. Secondary antibody goat anti-mouse total IgG HRP (1:2500 dilution) in blocking buffer was plated for 1 hour at room temperature. The plates were once again washed. The plates were developed for 30 seconds using TMB and quenched using 2N H_2SO_4. The absorbance at 450 nm was measured by plate reader. Serum Titers were generated using sigmoidal regression analysis on GraphPad Prism of Log10 serum dilution versus absorbance.

4.6 Hybridoma Development *(Conducted at CDC)*

The hybridoma fusions were conducted by the Immunodiagnostics Development team at CDC. Perfused B cells were mixed with SP2-IL6 myelomas and the cells were fused by electric-field induced cell-to-cell fusion. The fused hybridoma were then plated into a semi-solid matrix containing CloneDetect and picked for IgG positivity through automated selection.

4.7 Clonal Selection and Functionality Determination

Supernatant ELISA

Antigen specific antibody binding of hybridoma supernatant (containing secreted clonal IgG), was measured by streptavidin or protein ELISAs. Either 1 µg/mL streptavidin or 0.25 µg/mL of protein in 1x PBS was plated overnight at 4°C on high binding ELISA plates. The plates were then washed with 1x PBS with 0.05% tween (PBST). One hundred µL of casein blocking buffer was plated for 1 hour at room temperature with gentle shaking to prevent non-specific binding. The plates were subsequently washed with PBST. For the streptavidin ELISAs, cognate biotinylated antigen was then plated at a concentration of 0.25 µg/mL in blocking buffer for 1 hour at room temperature with shaking. The plates were then washed with PBST. Supernatant (100 µL) was plated directly onto the ELISA plate for 1 hour at room temperature. Secondary antibody goat anti-mouse total IgG HRP (1:2500 dilution) in blocking buffer was plated for 1 hour at room temperature. For the IgM and subclass ELISAs, anti-IgM, IgG1, IgG2a, IgG2b, or IgG3 HRP conjugates were plated instead of the total IgG HRP. The plates were once again washed. The plates were developed for 30 seconds using TMB and quenched using 2N H_2SO_4. The absorbance at 450 nm was measured by plate reader. Serum Titers were generated using sigmoidal regression analysis on GraphPad Prism of Log10 serum dilution versus absorbance.

K_d by BLI (Conducted at the CDC)

Antibody affinity constants were determined by the ImmunoDiagnostics team at the CDC. Label-free analysis of binding by biolayer interferometry (BLI) was performed for selected mAbs against their cognate antigen. The resultant data was analyzed to deduce direct binding affinities by the kinetic rate constants ($1/K_{ads} = k_{dis}/k_{on}$, where $1/K_{ads}$ = apparent equilibrium dissociation constant, k_{on} = association rate constant, and k_{off} = dissociation rate constant).

RESULTS AND DISCUSSION

5.1 Fentanyl Derivatives

5.1.1. Fentanyl Derivative Selection and Structures

We chose to target eight different fentanyl derivatives for mAb production including six commonly found in illicit use (fentanyl, fentanyl 13a, carfentanil, 4MeO-Bu fentanyl, 3Me-fentanyl, and acetyl αMe-fentanyl) and two metabolites that result from the breakdown of fentanyl in the body (norcarfentanil-1 and norcarfentanil-2). A recent study by Wharton, et al. (2021)[64] tested the efficacy of 19 commercially available immunoassays in detecting 30 common fentanyl derivatives. They found that while most were able to adequately detect a few compounds, none were capable of detecting a significant portion of the derivatives.[64] Additionally, some derivatives, notably 3Me-fentanyl and 4MeO-Bu fentanyl, were poorly detected across all commercially available immunoassays tested. Based on the need depicted by Wharton and team we selected our eight fentanyl derivatives for mAb development (Figure 1).

The synthesis of the propargylated fentanyl derivatives for vaccination and the biotinylated derivatives with PEG linker used in ELISA analysis was conducted by Dr. Minghao Xu in the lab of Prof. M.G. Finn at Georgia Tech (Appendix A). All derivatives include amide, anilidine, piperidine, and alkylbenzene functional groups except norcarfenanil-1 and norcarfentanil-2 (Figure 1). As metabolites that result from breakdown of fentanyl in the body, norcarfenanil-1 and norcarfentanil-2 increase in concentration over time after initial entrance of fentanyl into the body. This makes them valuable targets for blood and urine detection. Their small size and limited number of unique features, however, also poses a limit on the availability of unique epitopes for antibodies to bind. Based on these structural features we hypothesize that norcarfenanil-1 and

norcarfentanil-2 could be more difficult to elicit an optimal humoral immune response against than the other derivatives.

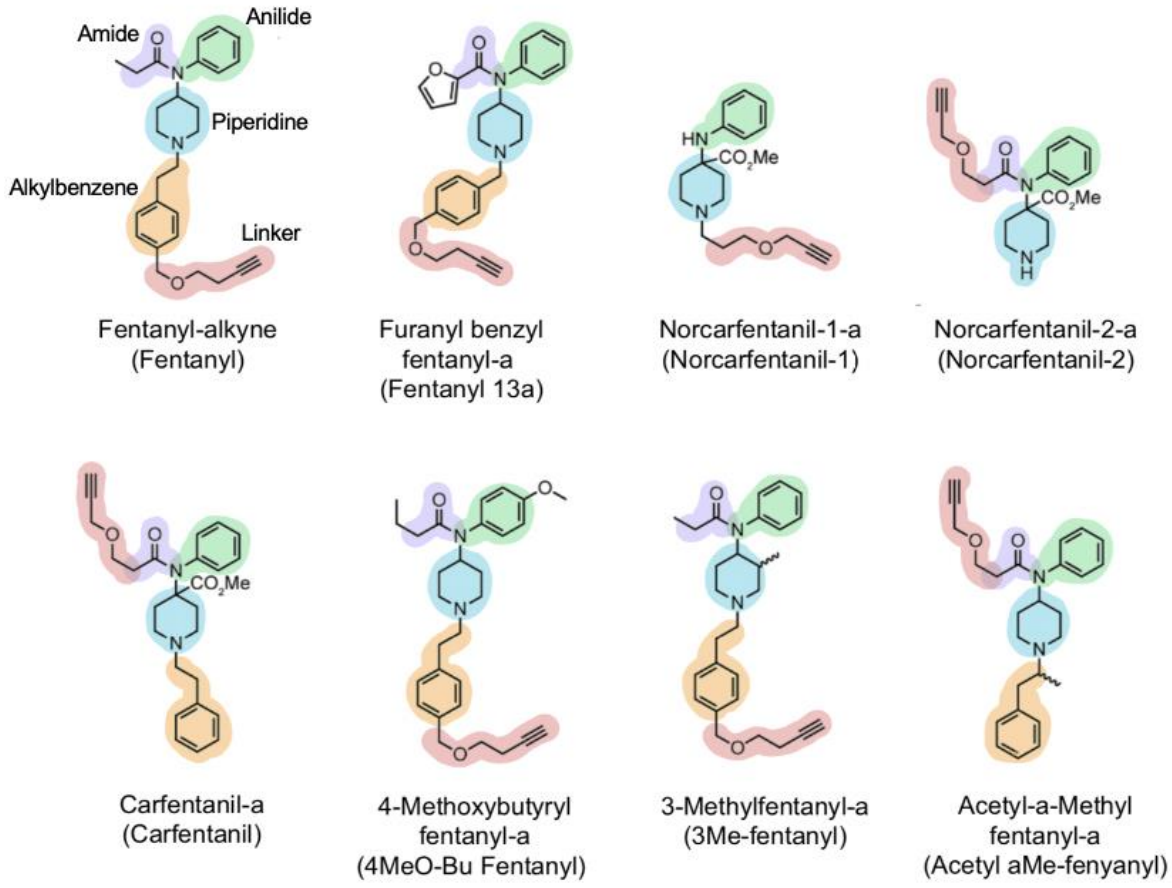

Figure 1. Structure of fentanyl derivatives for vaccine conjugates. Amide (purple) functional groups represented in all derivatives except fentanyl 13a. Anilide (green), piperidine (blue), and alkyne linker (red) group represented in all derivatives. Alkylbenzene (yellow) functional groups represented in all derivatives except norcarfentanil-1 and norcarfentanil-2.

Each derivative also has an alkyne linker installed for bioconjugation to the reactive azide linkers on the PP7 VLP particles by copper catalyzed azide-alkyne cycloaddition (CuAAC reactions and vaccine conjugation performed by Dr. Asheley Chapman). Fentanyl, fentanyl 13a, norcarfentanyl-1, 4MeOBu fentanyl, and 3Me-fentanyl each have the linker installed at the alkylbenzene "tail" position of the molecule (Figure 1). Norcarfentanil-1, carfentanil, and acetyl αMe-fentanyl have the linker installed at the amide "head" position of the molecule (Figure 1). The orientation of the "tail" linker allows more exposure for the amide anilide head of the molecule

while the “head” linker allows more exposure for the core of the molecule. This has the potential to affect the presentation of the molecules to BCRs and therefore influence the epitopes selected for in antibody production.

5.1.2. Immunization Strategy Optimization

Before immunizing mice with all the derivative vaccines, an optimization experiment was performed using the fentanyl 13a vaccine to determine optimal duration, appropriate number of boosts, and most effective adjuvant. Though VLPs are considered to be self-adjuvating, we chose to explore the potential benefit of the iNKT agonist PBS-57 (NKT) and TiterMax (TMX) adjuvants. Hapten vaccines have the tendency to overwhelm immune responses with IgM, decreasing the amount of class switching to the coveted high affinity IgG.[65, 66] Since both PBS-57 and TiterMax have been shown to direct humoral immunity to IgG production, we hypothesized that they may help to avoid this unwanted IgM influx.[29, 67] To test this hypothesis, we immunized BALB/c mice at week 0 with three immunization strategies: VLP-13a fentanyl vaccine alone (13a), 13a with the iNKT adjuvant (13a +NKT) and 13a with the TiterMax adjuvant (13a +TMX) (Figure 2A). The non-adjuvated group was boosted at weeks 2 and 4 and the adjuvated groups were boosted at week 6. All groups were then boosted again 3 days prior to termination and splenectomies were performed on week 13.

Serum ELISAs were conducted each week to determine antigen specific IgG antibody production (Figure 2B). All groups showed high titers ($>10^4$) beginning one week post initial immunization. Prior to week 6 the 13a +NKT group showed a slightly lower titer than the other groups, however, after the second immunization at week 6 it exceeded the other groups and had the highest titer upon termination, though the differences were not significant. These results show that a 13-week immunization schedule was unnecessary to produce a high antigen specific IgG

response. Though high titers were presented only one week post primary immunization, the ELISAs do not ensure high affinity antibody response, therefore it was determined that a 5-8-week immunization schedule with multiple boosts would be ideal to ensure adequate time for affinity maturation.

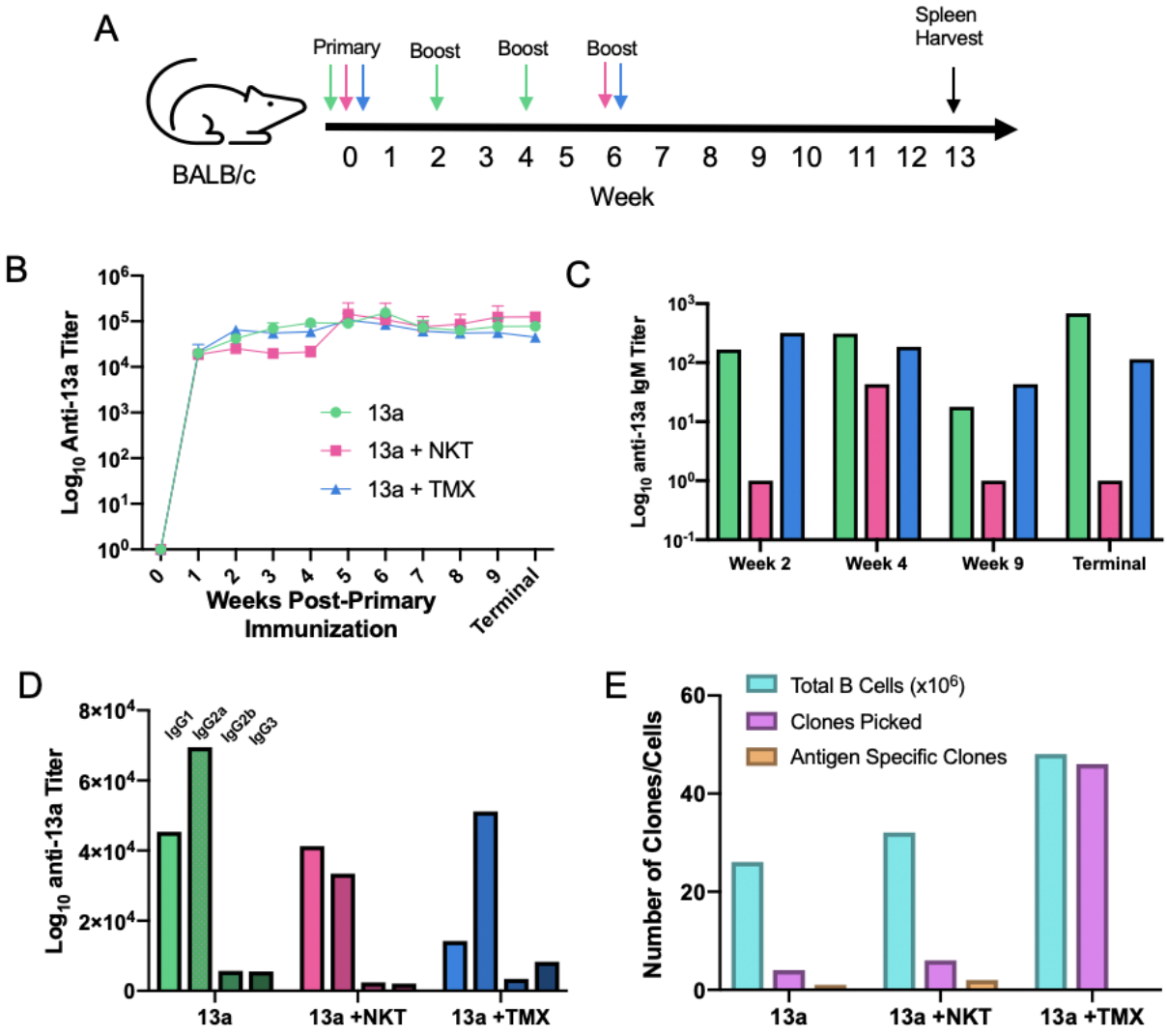

Figure 2. **Analysis of fentanyl 13a immunogenicity by adjuvant**. (A) Immunization schedule for PP7-fent 13a vaccine without adjuvant (green), with NKT agonist PBS-57 (pink) and with TiterMax (blue) in BAB/c. (B) Anti-fentanyl 13a IgG responses for each group measured by ELISA. Points represent mean and error bars are SEM (n=3 per group). (C) IgG isotype responses at week 9 for each group measured by ELISA. (D) IgM responses for each group at weeks 2, 4, 9 and 13 measured by ELISA. (E) Total number of B cells resulting from spleen perfusion (blue), number of IgG clones that resulted from hybridoma fusion (purple) and number of antigen specific clones from that population (yellow).

IgM titers were found by serum ELISA on weeks 2, 4, 9 and 13 to determine the potential for IgM overload, associated with hapten immunization[65, 66], among each adjuvant group (Figure 2C). The IgM titers for all groups each week were significantly lower than the IgG titers by an over 10^2 order of magnitude. The 13a and 13a +TMX groups showed similar trends where IgM titers stayed relatively constant between weeks 2 and 4 then fell post first boost and rose again by termination. The 13a +NKT group on the other hand, peaked at week 4 and subsequently fell following first boost, maintaining this low level through termination. While both the 13a and 13a +TMX groups showed IgM levels similar to each other throughout the immunization schedule, the 13a +NKT group had significantly lower IgM levels. None of the groups had high enough IgM levels relative to IgG levels to support the notion of IgM overload. Despite this, the very low IgM titers in the 13a +NKT group still support its use in ensuing experiments.

To provide evidence that affinity maturation had occurred, an IgG subclass analysis was performed by serum ELISA at week 9 (Figure 2D). BALB/c mice are capable of producing four IgG subclasses: IgG1, IgG2a, IgG2b, IgG3.[68] Each subclass has its own unique properties and path to development. Subclass switching from IgM to IgG1, IgG2a and IgG2b can occur through CD4+ T cell dependent cytokine release of IL-4, INF-γ and TGF-β respectively.[69] Since affinity maturation is associated with this cytokine induced class switching, high IgG1 and IgG2a levels by week 9 in all groups shows T cell dependent affinity maturation regardless of adjuvant. This result in the non-adjuvated 13a group is indicative of the self-adjuvating properties of VLPs which are able to promote T cell priming through activation of TLR7/8 by packed mRNA.[5] Studies have also shown in mice that IgG3 is formed mainly through a T cell independent process and is associated with early infection.[69] The low levels of IgG3 in all groups shows a highly developed IgG response by week 9. Subclass switching from IgG3 to IgG1 can also result from affinity

mediated switching.[70] Studies into the level of affinity maturation of each subclass in both mice and humans have shown that IgG1 tends to be the most affinity matured subclass since on average it has by far the most IGHV gene mutations.[71] While a high IgG2a response in each group is expected as it is associated with viral infection[6], it is notable that the 13a +NKT group is the only one that has higher IgG1 levels than IgG2a. This supports the literature which reports that NKT agonist adjuvants promote affinity mediated switching from IgG3 to IgG1.[67] The high levels of IgG1 and IgG2a, along with low levels of IgG3 at week 9 in each group supports the hypothesis that adequate affinity maturation has occurred to produce high affinity antibodies by week 9. Additionally, since IgG1 antibodies tend to have the highest affinity of the four subclasses, this data supports the use of NKT in subsequent experiments.

Since the immunizations for each group were performed in triplicate, at week 13 the mouse with the highest antigen specific titer from each group was selected for hybridoma development. Splenectomies were performed and the B cells perfused from the spleens. The number of B cells resulting from the perfusion were within normal range for all three groups (Figure 2E). The B cells were then electrofused with myeloma by the Immunodiagnostics Development team at the CDC. The number of IgG producing clones that resulted from the fusion was found to be significantly higher in the 13a +TMX mouse (46) than the 13a (4) and 13a +NKT (6) mice. Despite this, none of clones in this population were found to be antigen specific. On the other hand, the 13a population resulted in one antigen specific clone and the 13a +NKT population resulted in 2 antigen specific clones generated. The 13a +NKT clone population therefore had the highest antigen specificity rate of over 33%.

The results from this optimization experiment support a shorter 5-8-week immunization schedule with multiple boosts. This duration allows adequate time for high antibody response as

well as affinity maturation (Figure 2B,C&D). The multiple boosts aide in B cell differentiation and maturation. Since many of the results from the adjuvant groups were not significantly different from one another and a low sample size was used, no definitive conclusions can be made. Nevertheless, we chose to move forward with the NKT agonist as it resulted in the highest total IgG and IgG1 titers, the lowest IgM titers, and the most antigen specific clones.

5.1.3. All Derivative Immunizations

Vaccines were created for each of the eight fentanyl derivative targets by attaching the molecules to PP7 VLPs using the CuAAC reaction. The antigen density after installment on the VLP particles ranged from 100-228 fentanyl molecules per VLP depending on the derivative (Appendix A). This was an adequate number for proper multivalent display and no correlation was found between antigen density and ultimate serum antibody titers (Appendix A). Conjugates were purified by column chromatography and concentrated by centrifugation. Protein concentrations were determined by Bradford assay and characterization was confirmed by DLS, FPLC and LCMS (Appendix A).

After synthesis the vaccines were immunized into BALB/c mice at week 0 along with the NKT agonist with 4-7 replicate mice in each group. The mice were boosted at weeks 2 and 4 as well as 3 days prior to termination which ranged from week 5-8 (Figure 3A). Mice were bled at one-week intervals and serum ELISAs were conducted to determined antigen specific IgM and IgG binding over the course of the immunization schedule. Similar to the trend shown by the 13a +NKT group in the optimization experiment, IgM titers were extremely low compared to IgG titers and peeked at about 3 weeks. Even the acetyl αMe-fentanyl immunized mice, which had the

highest week 3 IgM titers, also had very high IgG titers (>10^4) by week 3. This is a positive sign that IgM overload due to the hapten vaccine was not occurring.

Similarly to the optimization experiment, most vaccines resulted in high titers (>10^4) only 1 to 2 weeks post primary immunization (Figure 3B). This was not the case for norcarfentanil-1 and norcarfentanil-2. As previously hypothesized, both these immunogens resulted in a lower humoral immune response that the other derivatives (Figure 3C). Both norcarfentanil-1 and norcarfentanil-2 were able to steadily increase titers over the course of the immunization schedule.

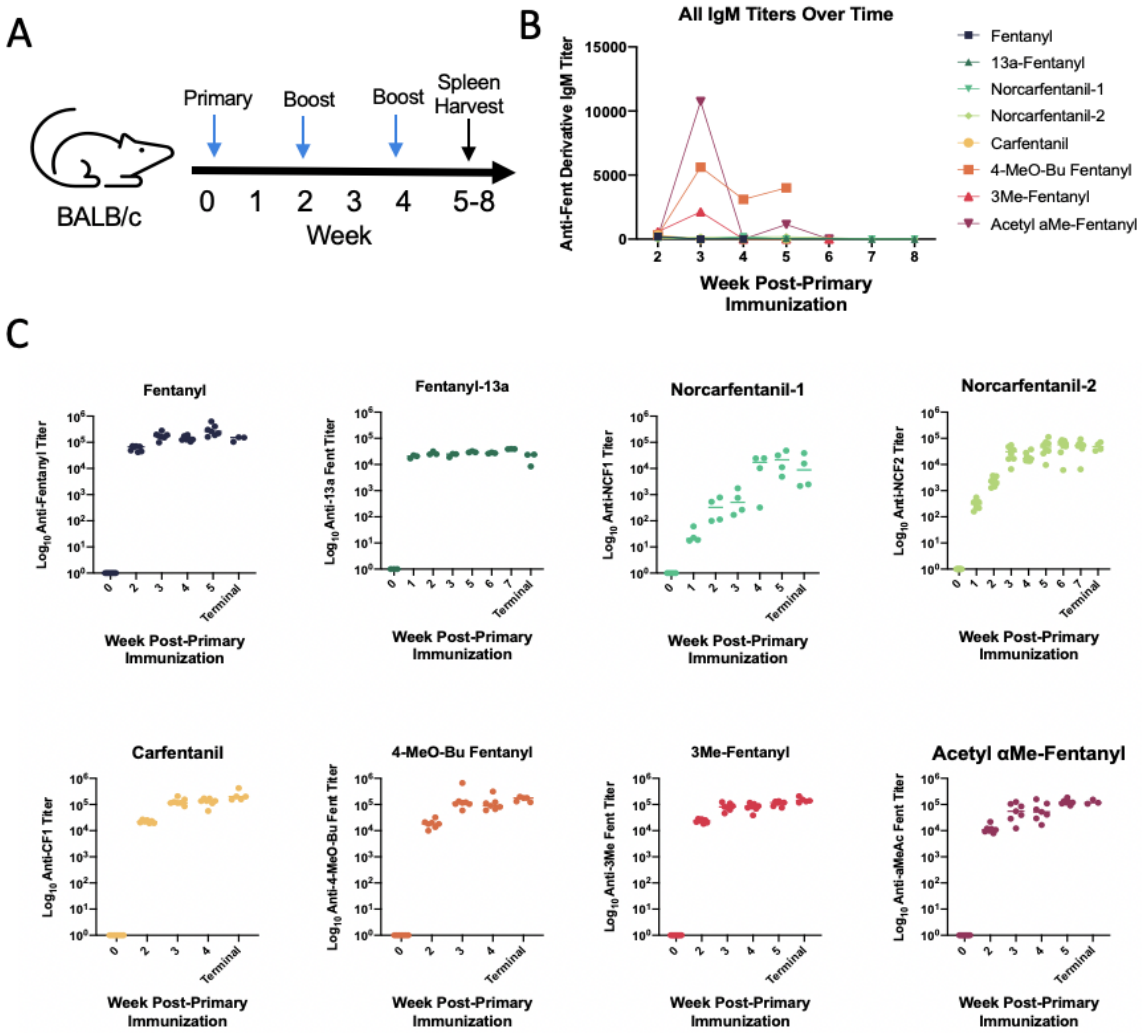

Figure 3. Immunogenicity of eight fentanyl derivative VLP-conjugate vaccines. (A) Immunization schedule of BALB/c mice with fentanyl derivative VLP vaccines and NKT agonsit. (B) Anti-cognate antigen IgM titers determined by ELISA. (C) Anti-cognate antigen IgG titers over time determined by ELISA. Means show by line and individual mice depicted as dots.

Norcarfentanil-2 mice were able to climb to a titer of nearly 10^5 which is on the same order of magnitude as the other vaccines. Norcarfentanil-1 immunized mice, however, were only able to an average titer of 10^4, about one order of magnitude smaller than the rest, by termination. These results show that the vaccine for each derivative was able to produce strong antigen specific humoral immune response, a promising step towards mAb development.

5.1.4. Hybridoma Fusion and Clone Characterization

At week 5-8 depending on immunization schedule the mouse with the highest antigen specific titer was from each of the vaccine groups was selected for hybridoma development. Splenectomies were performed and the B cells perfused from the spleens. The number of B cells resulting from the perfusion were within normal range for all fusions (Appendix A). The B cells were then electrofused with myeloma by the Immunodiagnostics Development team at the CDC.

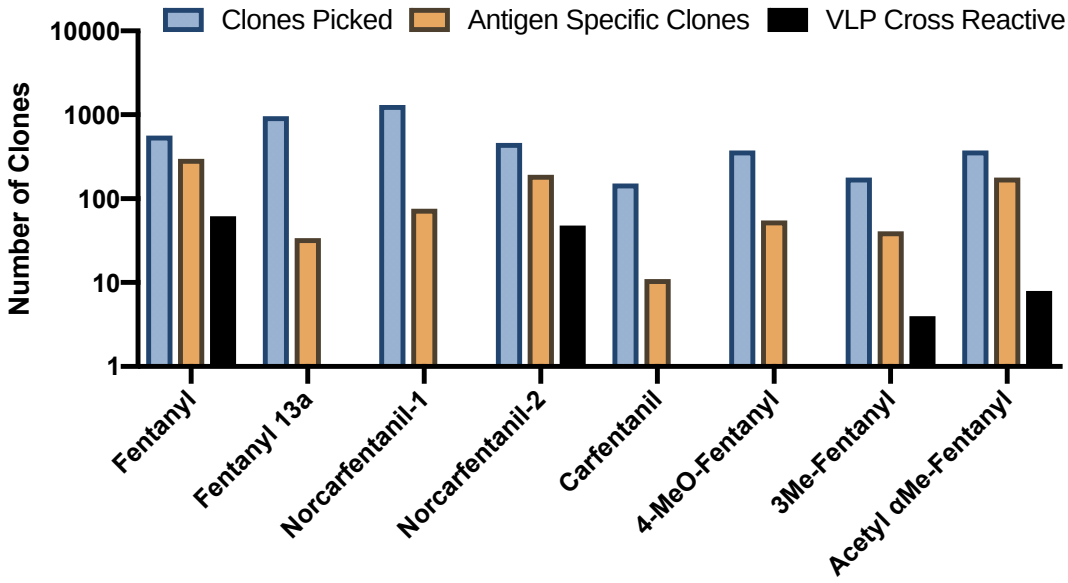

Figure 4. Analysis of fentanyl hybridoma fusion statistics. Number of IgG clones that resulted from hybridoma fusion (blue), number of antigen specific clones from that population (yellow), and number of antigen specific clones also cross reactive to PP7(black).

The hybridoma were screened for IgG production (clone picked), antigen specificity and the antigen specific clones for VLP cross reactivity (Figure 4). The number of IgG producing clones that resulted from the fusion ranged from 152 (carfentanil) to 1316 (Norcarfentanil-1). The number of antigen specific clones ranged from 11 (carfentanil) to 299 (fentanyl). All groups resulted in significantly more positive clones with the optimized immunization schedule than the 13-week schedule. Only fentanyl and norcarfentanyl-1 had a large number of VLP cross reactive clones of those shown to be antigen specific with 62 and 48 respectively. VLP cross reactivity is an indicator of hapten-peptide presentation on MHC II. The norcarfentanil-1 and norcarfentanil-2 clones were dropped from further experimentation due to a low probability of high affinity antibodies as previously discussed.

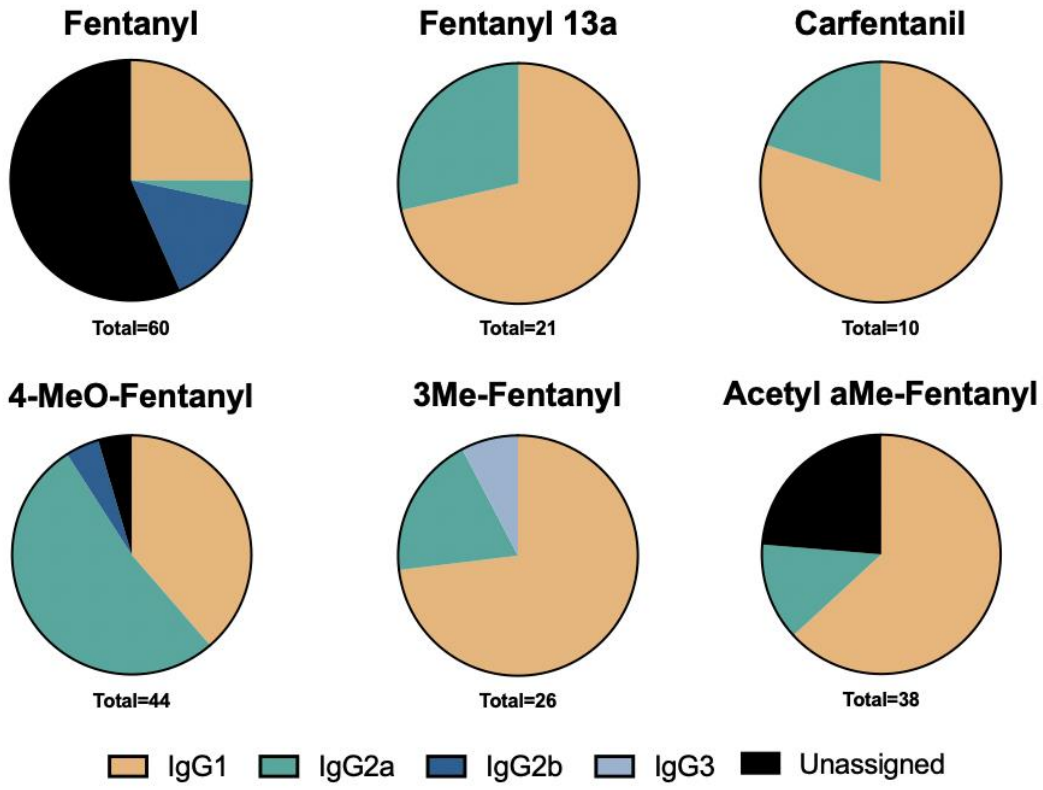

Figure 5. Subclass determination of fentanyl derivative mAb supernatant. IgG subclass of antigen specific clones determined by supernatant ELISA analysis. Unassigned labeled for multiple positive subclasses.

An IgG subclass analysis was run by supernatant ELISA to determine the subclass of antigen specific clones (Figure 5). Cloned were labeled as unassigned if multiple subclasses were found within a single clonal line's supernatant. This was found in clones within the fentanyl, 4-MeO-fentanyl and acetyl αMe-fentanyl groups. All groups had mAbs with both IgG1 and IgG2a subclasses. This is consistent with the 13a +NKT serum results from the optimization experiment, in which these subclasses had the highest titers. IgG2b and IgG3 mAbs also resulted from the 4-MeO-fentanyl and 3Me-fentanyl immunizations respectively. The high percent of IgG1 subclasses across all derivatives is indicative of the success of the vaccine platform for hapten immunizations.

5.1.5. MAb Functionality

The supernatant from clones that were positive for binding to their cognate antigen were then tested by ELISA for cross-reactivity to the other seven derivatives (Appendix A). The absorbances were normalized to binding against their respective immunogen as a percentage across all 180 mAbs tested with 100% representing the highest absorbance and strongest binder, and 0% representing the lowest absorbance and no binding. The binding patterns of each mAb were compared and 14 unique binding patterns were found. The mAbs with the highest percent binding to their positive matches and lowest percent binding to their negative matches were chosen to represent each binding pattern group (Figure 6). In this way, we hope to capture representative mAbs capable of distinguishing between these compounds in immunoassays.

Interestingly, all of the mAbs that showed the most distinct binding for each binding pattern group were derived from only three immunizations: acetyl αMe-fentanyl (αMe), fentanyl (82), carfentanil (CF1). αMe-10H2 was the only mAb found to positively differentiate one derivative (acetyl αMe-fentanyl) from all other derivatives. This mAb's ability to distinguish the acetyl αMe-

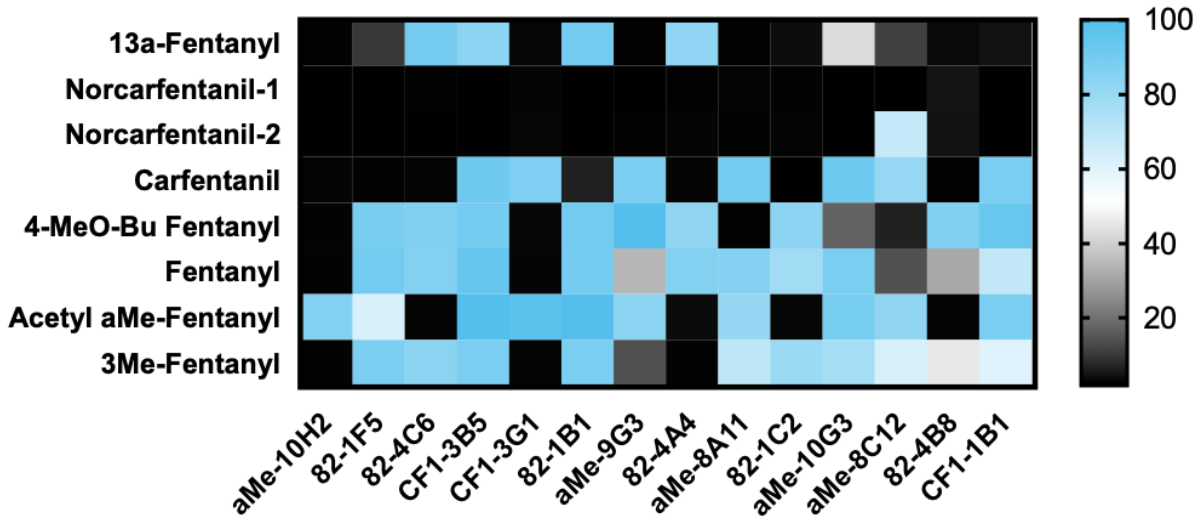

Figure 6. Cross reactivity of mAbs to eight fentanyl derivatives. Percent binding of 14 mAbs representing unique binding patterns for cross reactivity to the eight fentanyl derivatives.

fentanyl from the fentanyl molecule as well as from the carfentanil which it shares a linker location with, makes it highly likely that the α-methyl functional group on the ethylbenzene plays a significant role in the epitope binding as that is the only differentiating structure. Unsurprisingly, the mAbs did not bind norcarfentanil-1 or norcarfentanil-2 well since these metabolites have far fewer functional groups to bind than the other derivatives. In fact, the only mAb capable of binding either was αMe-8C12 which only bound norcarfentnail-2. The ability of this mAb to bind norcarfentanil-2, but not norcarfentanil-1 could be due to the presentation of acetyl αMe-fentanyl vaccine from which the mAb was derived, which has a "head" linker location similar to norcarfentanil-2 as opposed to norcarfentanil-1 which has a "tail" linker location. The other possible explanation for this is that the mAb binding relies heavily on the amide functional group, which is not present on norcarfentanil-1. Another interesting binding pattern is that of 82-1B1. This mAb did not show binding to carfentanil but did to acetyl αMe-fentanyl. A possible explanation for this is that the region between the piperidine and anilide plays an important role in the mAb's binding, and the CO_2Me group interferes with this. This is consistent with the mAb's lack of binding to norcarfentanil-1 and norcarfentanil-2, which both also have the CO_2Me group.

The binding pattern of CF1-3G1 is interesting in that it is most likely not due to specificity to acetyl αMe-fentanyl and carfentanil, but rather due to limitations in the ELISA design which places a PEG linker on the alkyl benzene of the other four non-metabolite derivatives, thereby blocking a probable binding site of the mAb. The various binding patterns of these mAbs once tested against unmodified fentanyl analogs (not possible in our lab) could shed further light on the important functional groups for binding corresponding and help inform future vaccine design for epitope targeting.

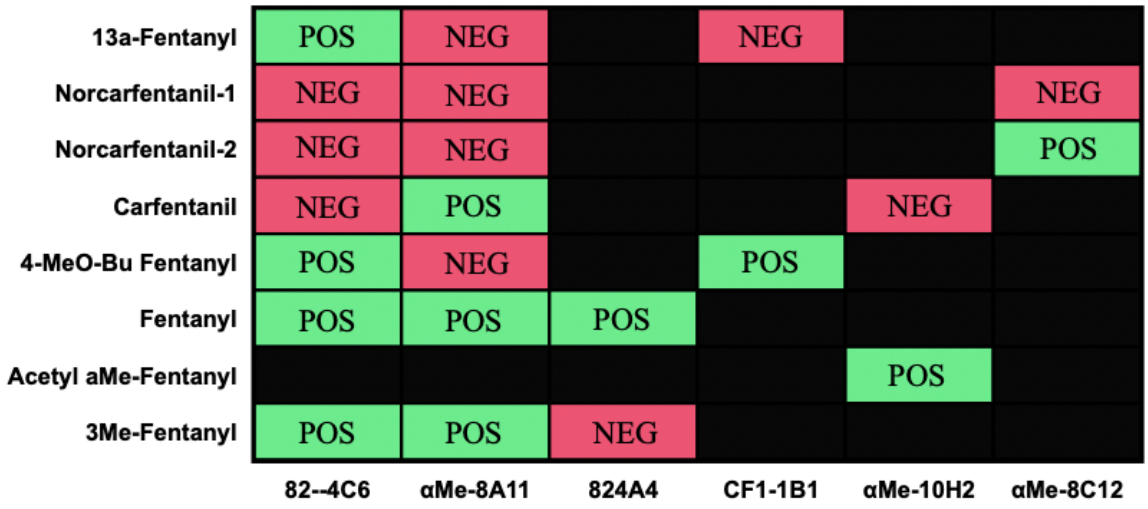

Figure 7. Distinguishing derivatives using mAbs. Differential binding of six mAbs to the eight derivatives needed to positively distinguish each derivative from all others (except norcarfentanil-1).

Of the 14 mAbs selected for their unique binding pattern, only 6 (82-4C6, αMe-8A11, 82-4A4, CF1-1B1, αMe-10H2 and αMe-8C12) are needed to positively distinguish each derivative from the others excluding norcarfentanil-1 (Figure 7). The derivatives were first able to be split into two groups based on positive or negative binding to 82-4C6. From there these two groups were each able to be split again based on positive or negative binding to αMe-8A11. The resulting groups of two derivatives were then able to be distinguished using four additional mAbs: 13a fentanyl from 4-MeO-Bu fentanyl with CF1-1B1, norcarfentanil-1 from norcarfentanil-2 with αMe-8C12, carfentanil from acetyl αMe-fentanyl with αMe-10H2, and fentanyl from 3Me-

fentanyl with 82-4A4. Though validation of binding using unmodified derivatives must still be conducted to ensure no linker effect on the ELISA cross reactivity results, this data shows that together these six mAbs can be used as a diagnostic tool to differentiate among these eight derivatives.

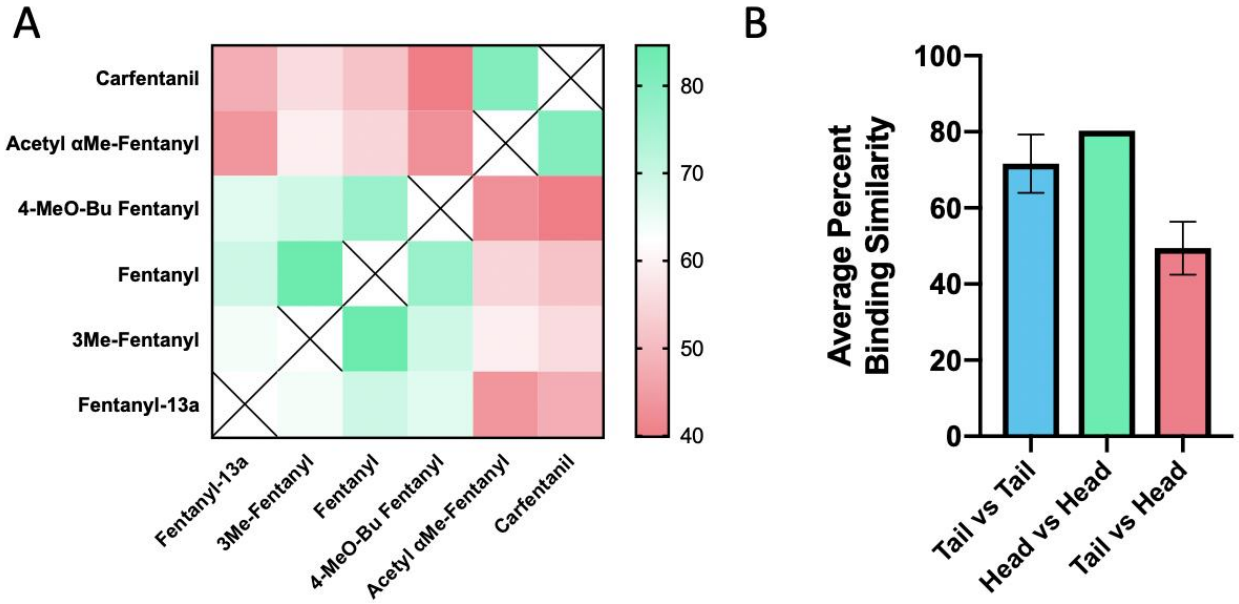

Figure 8. Analysis of linker location effect on fentanyl mAbs. (A) Average percent binding similarity between each derivative determined by subtracting the average difference in percent binding of each derivative comparison across the 14 mAbs with different binding patterns from 100%. (B) Average percent binding similarity averaged across all tail vs tail linker (n=6), head vs head linker (n=1), and tail vs head linker (n=8) comparisons.

The linker location effect on both the immunology of molecule display by the VLP and the ELISA results from use of the PEG linker was further analyzed. The similarity in the percent binding between the six non-metabolite derivatives to the 14 mAbs with different binding patters was determined (Figure 8A). There is a clear distinction between binding of the derivatives with "head" linkers (carfentanil and acetyl αMe-fentanyl) and the other four with "tail" linkers. This distinction was summarized to show the average percent binding similarity of all "tail" linker derivatives compared to "tail" linker derivatives, "head" linker derivatives compared to "head" linker derivatives, and finally "tail" linker derivatives compared to "head" linker derivatives (Figure 8B). A Kruskal-Wallis test with Dunn's multiple comparison was run to determine if the

differences between each group were significant and the results showed the “Tail vs Tail” group was significantly greater in average percent binding similarity than the “Tail vs Head” group. The “Head vs Head” group was not significantly greater, however since it actually had a higher average percent binding similarity than even the “Tail vs Tail” group this can be attributed to the fact that there was only one value within this group.

This difference in binding similarity can be attributed to two factors: the epitope targeting of the antibodies due to display orientation of the molecule on the VLP, and the location of the PEG linker on the molecules for ELISA analysis most likely blocks epitopes. The epitope targeting is advantageous to the study because it shows that by adjusting linker location, we are able to better target differentiating functional groups. The PEG linker on the molecules for ELISA analysis, however, complicates these results. It is likely that the mAbs such as CF1-3G1 require the alkylbenzene functional group for binding. This means this mAb is probably also capable of binding all six derivatives, the ELISA results just show otherwise because the PEG linker sterically inhibits this binding on the tail linker molecules. This shows limitations in our analytical strategy for mAb cross reactivity between molecules with different linker locations.

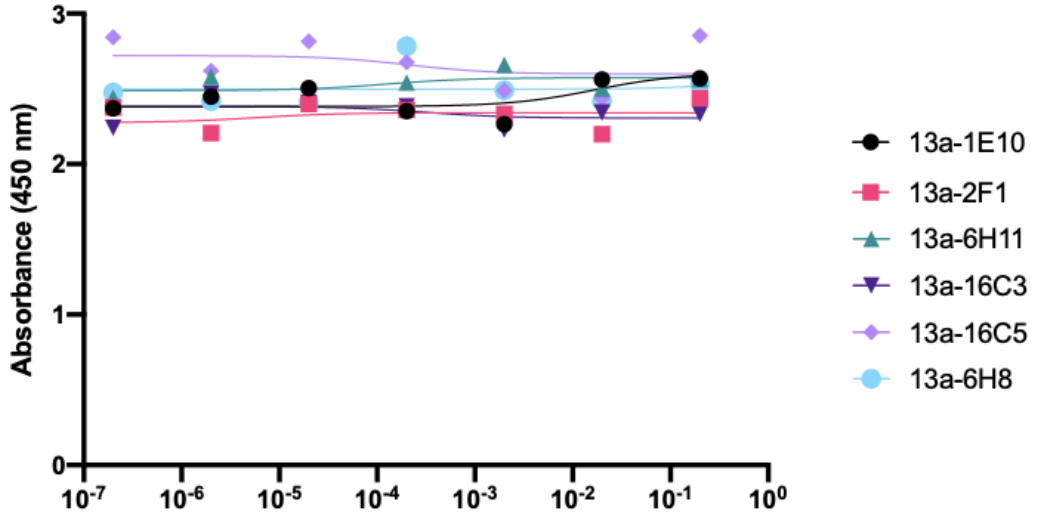

Figure 9. Cross reactivity of fentanyl 13a mAbs to naloxone. Effect of introduction of varying concentrations of naloxone to mAb binding of fentanyl-13a determined by ELISA.

In addition to use in diagnostics, anti-fentanyl mAbs also have the potential to be humanized and used as overdose therapeutics as previously described by Smith et al.[48] In this model naloxone would be used as the fast acting treatment and mAbs has the longer term treatment after admission to a hospital. This makes it important that the mAbs have no cross reactivity to the naloxone that could dampen both treatments effects. To ensure this we analyzed the competitive binding ability between naloxone and fentanyl-13a to six anti-13a mAbs (Figure 9). Decreasing concentrations of naloxone beginning at nearly 1 M (at the maximum solubility concentration) were mixed with the biotinylated fentanyl 13a and the relative binding was determined. The results showed that naloxone did not inhibit mAb binding to fentanyl-13a, nor did the naloxone bind the mAb to any appreciable amount. This shows that when used as a combination therapy for overdose victims these two treatments could be used in tandem with no interference.

5.1.6. Conclusions and Future Experimentation

Here, we demonstrated that a VLP conjugate vaccine platform can be used to develop mAbs for certain fentanyl derivative. We found the optimal vaccine strategy is a short 5-8-week immunization schedule using an NKT agonist as the adjuvant. Under these conditions we were able to elicit a high titer polyclonal antibody response against each of the derivatives. We were then able to isolate 14 mAbs with unique binding patters to the eight fentanyl molecules. Together 6 of these mAbs can be used to positively differentiate between all fentanyl molecules tested except norcarfentanyl-1. One mAb (αMe-10H2) was able to exclusively bind acetyl αMe-fentanyl, allowing it to differentiate this derivative from all others tested. We also demonstrated in an early experiment that mAbs have the potential to be used in conjunction with naloxone as an overdose

treatment, which can be further explored how by measuring rate of fentanyl clearance in mice in future experiments.

To validate the differential binding of these mAbs to the fentanyl derivatives, we will have to analyze their binding to the unmodified fentanyl derivatives as the linkers have the potential to limit binding in our current analytical method. It is also important to ensure these antibody-molecule interactions are high affinity. To do this, binding affinities will be determined by BLI. The chosen mAbs from based on results from these experiments will be sequenced. Lastly, to move forward with potential therapeutic use, the chosen mAbs would need to be tested to ensure they do not have any binding interactions with naloxone.

5.2 SARS-CoV-2 Peptides

5.2.1. Peptide Selection and Structures

We chose to target six different SARS-CoV-2 peptides based on known neutralizing activity of the epitopes and probability of binding MHC II. Peptides 6 and 9, each part of the RBD of the spike protein, were cloned into the PP7 plasmids as C terminal extensions (Figure 10). Peptides 16 and 17, part of the C terminal domain and N terminal domain respectively, were also genetically conjugated as C terminal extensions of the PP7 plasmid. An RBM peptide containing 4 out of 6 RBD/ACE2 contact residues[52] (RBM) and the spike protein fusion peptide (FP) were chemically ligated to the PP7 assembled particles using CuAAC.

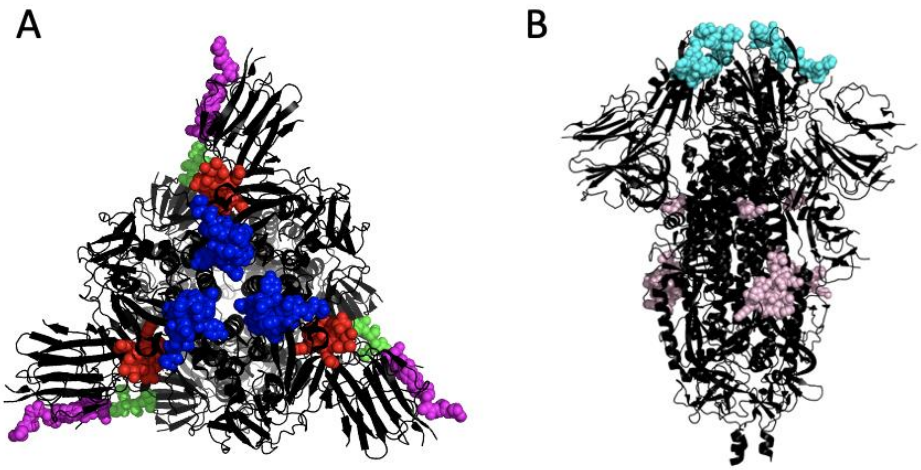

C

Peptide	Modification	Sequence	Start Residue	End Residue	S1 Region
6	Genetic	LFRKSNLKPFERDIS	455	470	CTD - RBM partial
9	Genetic	SYGFQPTNGVGYQPY	494	508	CTD - RBM partial
16	Genetic	QTNSPRRARSVASQ	677	692	CTD partial
17	Genetic	FHAIHVSGTNG	61	76	NTD partial
RBM	Ligated	FNCYFPLQSYGFQPTN	486	501	RBM
FP	Ligated	SFIEDLLFNKVT	812	855	FP1 partial

Figure 10. Structure of SARS-CoV-2 peptides for vaccine conjugation. (A) Top view of cartoon SARS-CoV-2 spike protein (6vxx) with sphere peptides 6 (red), 9 (blue), 16 (green) and 17 (purple). (B) Side view of cartoon SARS-CoV-2 spike protein with sphere peptides RBM (light blue) and FP (pink). (C) Table of each peptide with type of modification used for VLP attachment, sequence, and location.

5.2.2. Peptide Immunizations

The immunizations were split into three groups with different immunization schedules. All groups were first given a primary immunization with the PP7-peptide conjugate vaccine followed by three boosts with either an mFc tagged RBD or the ectodomain spike homotrimer glycoprotein. We hypothesized that the primary dose would target the immune response toward the peptide of interest and the boosts would select for those that also bound the peptide in its correct confirmation.

The first group received either peptide 6 conjugate vaccine (PP7-covid-6) or the peptide 16 conjugate vaccine (PP7-covid-16). They were both given a primary immunization with the conjugate vaccine followed by whole protein boosts at weeks 2, 3, and 4 (Figure 11A). The anti-ecto titer remained low for the PP7-covid-6 mice at week 3 but increased to almost 10^3 by termination (Figure 11B). Though lower than expected, the titer was considered adequate for scheduled splenectomy and B cell extraction 3 days following the final boost. The PP7-covid-16 mice anti-ecto titers steadily increased to a robust final terminal titer ($>10^4$).

The second group received one of two conjugate vaccine cocktails for primary immunization. This strategy allows for targeting of multiple epitopes in a single vaccination. Cocktail 1 contained an equal mixture of PP7-covid-6, PP7-covid-16 and PP7-covid-17. Cocktail 2 contained an equal mixture of PP7-covid-6 and PP7-covid-9. All of these conjugated were made through genetic modification of the PP7 plasmid (Figure 10). Following primary immunization, all mice were boosted with whole protein RBD on weeks 2, 4, and 8 (Figure 11A). The Cocktail 1 mice, similar to the PP7-covid-6 mice showed low anti-ecto titers through week 4, then increased to $>10^4$ by termination (Figure 11B). The cocktail 2 mice, similar to the PP7-covid-16 mice, already had high anti-ecto titers by week 4 and continued to increase to $>10^4$ by termination.

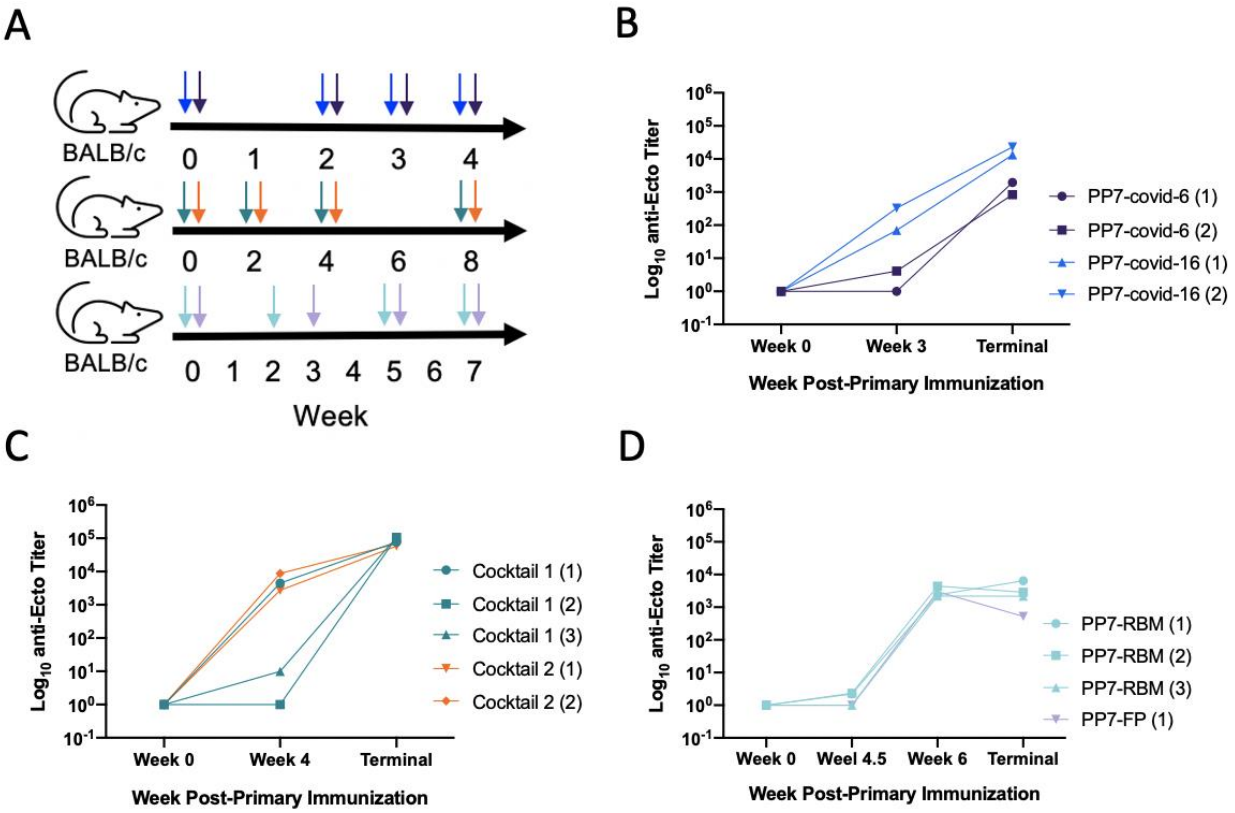

Figure 11. Immunogenicity of SARS-CoV-2 peptide VLP-conjugate vaccines. (A) Immunization schedule for each vaccine group PP7-covid-6 (blue), PP7-covid-16 (purple), Cocktail 1 (green), Cocktail 2 (orange), PP7-RBM (light blue), PP7-FP (purple). (B) Anti-ecto titer over time of genetically modified peptide groups determined by ELISA. (C) Anti-ecto titer over time of cocktail peptide groups determined by ELISA. (D) Anti-ecto titer over time of chemically modified peptide groups determined by ELISA.

The third group received primary immunizations with either the RBM or FP peptide that were both presented by covalent chemical modification of the PP7 particles post assembly. Following primary immunization, the PP7-RBM mice were boosted with whole protein RBD at weeks 2, 5, and 7 and the PP7-FP mice at weeks 3, 5, and 7 (Figure 11A). Mice from both immunization types showed low titers at week 4.5 which then increased to about 10^4 by week 6 and maintained those titers at termination. This is a similar trend to those showed by the PP7-covid-6 and Cocktail 1 immunizations.

We hypothesized that the reason for low anti-ecto titers post immunization with the VLP-peptide, but a large increase after immunization with whole protein could be a result of one of two

immunological factors. First, the linear display of the peptides on the PP7 could be inadequate to create an immune response against the peptides in their confirmation as part of the whole ectodomain. This hypothesis would mean we were unsuccessful at directing the immune response to that peptide and the later increase in titer was due solely to an untargeted immune response at the whole protein. The other explanation for the trend shown is that the VLP-peptides were able to initiate the targeted immune response, but that proliferation of those B cells did not occur until introduction of the whole protein. This hypothesis would support the conclusion that we were able to direct the immune response towards the peptide of interest. To further assess this heterologous prime-boost strategy we designed an experiment targeting mutant peptides described in the Mutant Peptide section of this chapter.

5.2.3. Hybridoma Fusion and Clone Characterization

Though we could not validate that the polyclonal mouse immune response was directed towards the peptides of interest we chose to move forward with hybridoma development. Splenectomies were performed 3 days post final boost and the B cells perfused from the spleens. The number of B cells resulting from the perfusion were within normal range for all fusions (Figure 12). The B cells were then electrofused with myeloma by the Immunodiagnostics Development team at CDC. The IgG producing hybridoma were then picked and screened for binding to the whole spike ectodomain. From the first group of immunizations, PP7-covid-6 and PP7-covid-16 resulted in 192 and 2 clones respectively that bound the ectodomain (Figure 12A). From the second group of immunization, Cocktail 1 and Cocktail 2 resulted in 71 and 13 clones respectively that bound the ectodomain (Figure 12B). From the third group, PP7-RBM and PP7-FP resulted in 6 and 25 clones respectively that bound the ectodomain (Figure 12C).

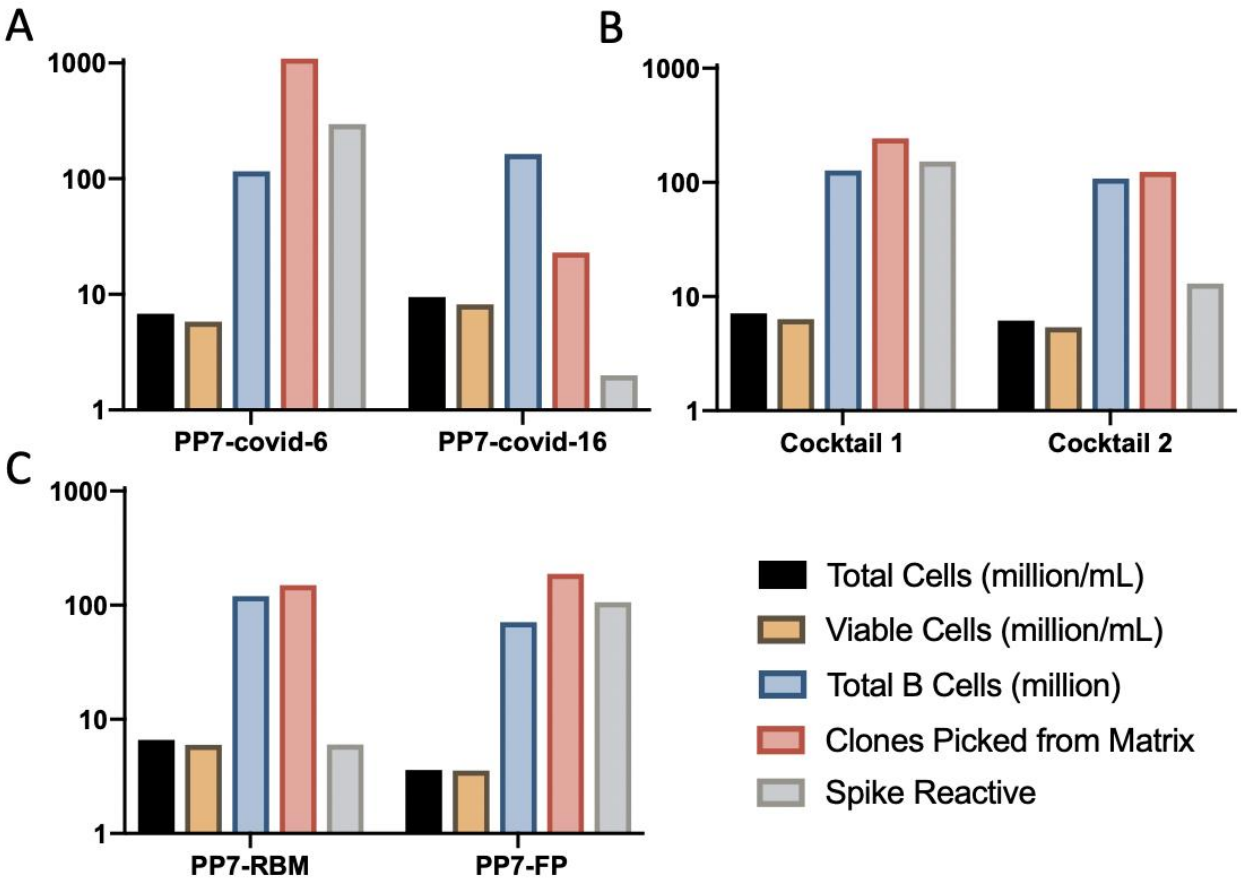

Figure 12. Statistics from SARS-CoV-2 peptide fusions. Number of cells perfused from spleens per mL (black), number of cells still alive by time of experiment per mL (yellow), total number of B cells perfused from spleens (blue), total number of IgG producing hybridoma (pink), total number of hybridoma producing spike reactive IgG (grey).

The data analysis is limited by the analytical methods of epitope mapping and therefore conclusions about mechanisms cannot be made between immunization groups. Nevertheless, it is notable that within the first two groups in which each immunogen showed different trends in anti-ecto titer development, the immunogen with lower post primary immunization titers (PP7-covid-6 and Cocktail 1) resulted in more spike reactive clones than its partner immunogen that followed the same schedule. This would make the hypothesis that the linear peptide display was unable to produce a directed B cell response that could be further proliferated with the whole protein unlikely. This is because a later introduction of the ecto, especially in the case of the first immunization group which saw whole protein for the first time only two weeks before termination,

would likely result in fewer anti-ecto IgG as IgG response takes time to mount. These results are promising sign that the VLP-peptide primary immunization did direct an initial peptide specific immune response.

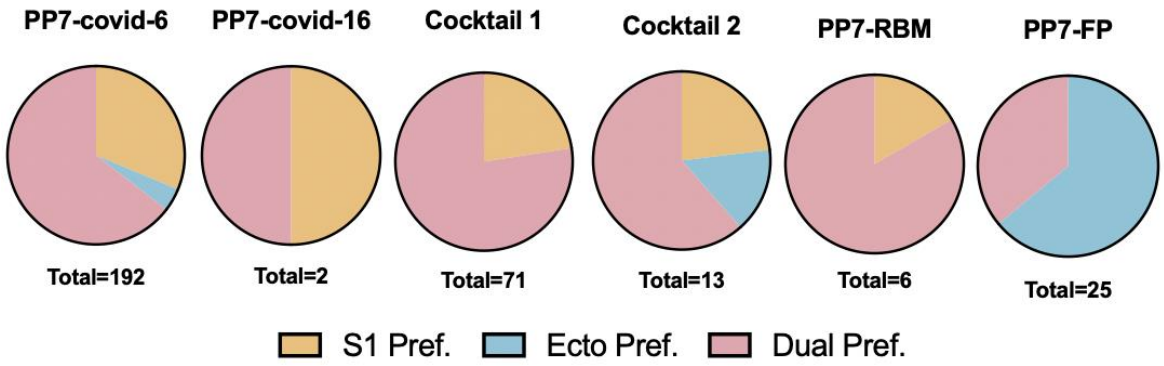

Figure 13. Binding preference of SARS-CoV-2 peptide mAbs preference. Breakdown of binding preference of each clone to either S1 (yellow), Ecto (blue), or both (pink) determined by ELISA.

Though it is difficult to determine exact epitope targeting of antibodies without a cryo-EM structure of their binding, the breakdown of our mAbs binding to the S1 subunit versus the entire ectodomain does provide some insights (Figure 13). The S1 subunit (residues 14-685)[33] contains peptides 6, 9, 17, RBM, and part of 16. The FP is the only peptide tested that lies completely outside of the S1 subunit.[72] We analyzed the binding of each mAb to both the whole ectodomain and the S1 subunit by ELISA to determine if it had a preference for one or bound both. The dual preference mAbs likely bind somewhere on the S1 subunit since this is also on the ectodomain. Those with an ectodomain preference likely bind outside of the S1 subunit.

The FP has by far the highest percentage of ectodomain preferred mAbs, however this trend could be a result of this immunization receiving whole ectodomain boosts rather that S1 and RBD boosts rather than true epitope targeting. The ectodomain preferred mAbs from the PP7-covid-6 and Cocktail 2 are surprising considering neither none of the immunizations these mAbs are derived from used any protein outside the S1 subunit. This data does not provide information on exact epitope targeting; however, it does narrow down the likely binding domains of each mAb.

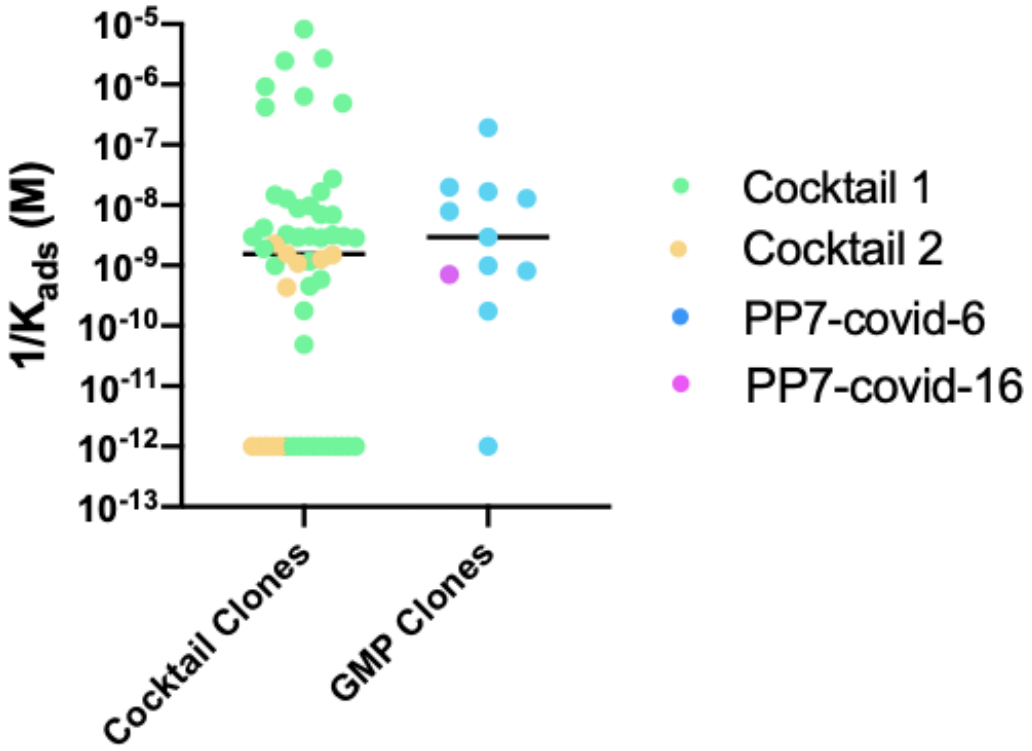

Figure 14. Binding affinities of SARS-CoV-2 peptide mAbs. binding affinities depicted as $1/K_{ads}$ for mAbs determined by BLI.

In order to be used in diagnostics or as biological reagents, it is important that the mAbs not only bind the antigen of interest but also bind it with a high affinity. The Immunodiagnostics Development team at the CDC determined the binding affinity of chosen clones by BLI (Figure 14). Multiple mAbs were found to have exceptional nanomolar and sub-nanomolar affinities for the ectodomain, ideal for use in diagnostics. Multiple mAbs from the Cocktail 1 and Cocktail 2 immunizations as well as one from the PP7-covid-6 immunization had picomolar binding affinities, however this is likely below the instruments limit of detection so exact affinities cannot be determined. This confirms that the immunization schedule was successful in eliciting a humoral immune response that allowed for B cell affinity maturation and therefore a high affinity IgG response.

5.2.4. Mutant Peptides

Based on the early successes with peptide targeting with known neutralizing peptides on the spike protein, we also began experiments to try to target high profile mutations. Our first target was the Y453F mutation in the spike protein RBD. We designed a heterologous prime-boost strategy to determine the best immunization strategy for peptide targeting. The VLP-peptide vaccines were made with PP7 using the CuAAC reaction to attach either the wild type or mutant linear peptide. The two immunization strategies were a) prime with wild type or mutant VLP-peptide and boost twice with wild type or mutant whole RBD protein or b) prime with wild type or mutant whole RBD protein and boost twice with wild type or mutant VLP-peptide (Figure 15A). For each schedule, 5 mice were immunized with prime and boosts on weeks 0, 2, 4 and the mice were terminated at week 7 for hybridoma production. The serum was monitored throughout for anti-RBD and anti-peptide IgG response by ELISA.

Both the wild type and mutant immunizations showed similar trends for the two different schedules. For schedule a, both immunizations initially showed a sharp increase in anti-peptide response at week 2 to a titer of nearly 10^4 followed by a steady decline (Figure 15B, 15C). The initial anti-RBD response for each was low before receiving whole protein boosts at week 2 and then steadily increased to a titer of about 10^5. The decrease in anti-peptide response corresponding to the increase in RBD response could indicate that the initial peptide immunization was not enough to direct the immune response post RBD immunization towards the peptide. As a result, the immune system seems to have been overwhelmed by the immunogenicity of the RBD creating a response to many epitopes on the protein. This especially seems to be true with the 1a immunization as the week 7 peptide titer dropped nearly to pre-immunization levels. Even in the 2a immunization the peptide response at week 7 was 3-fold lower than the total RBD response.

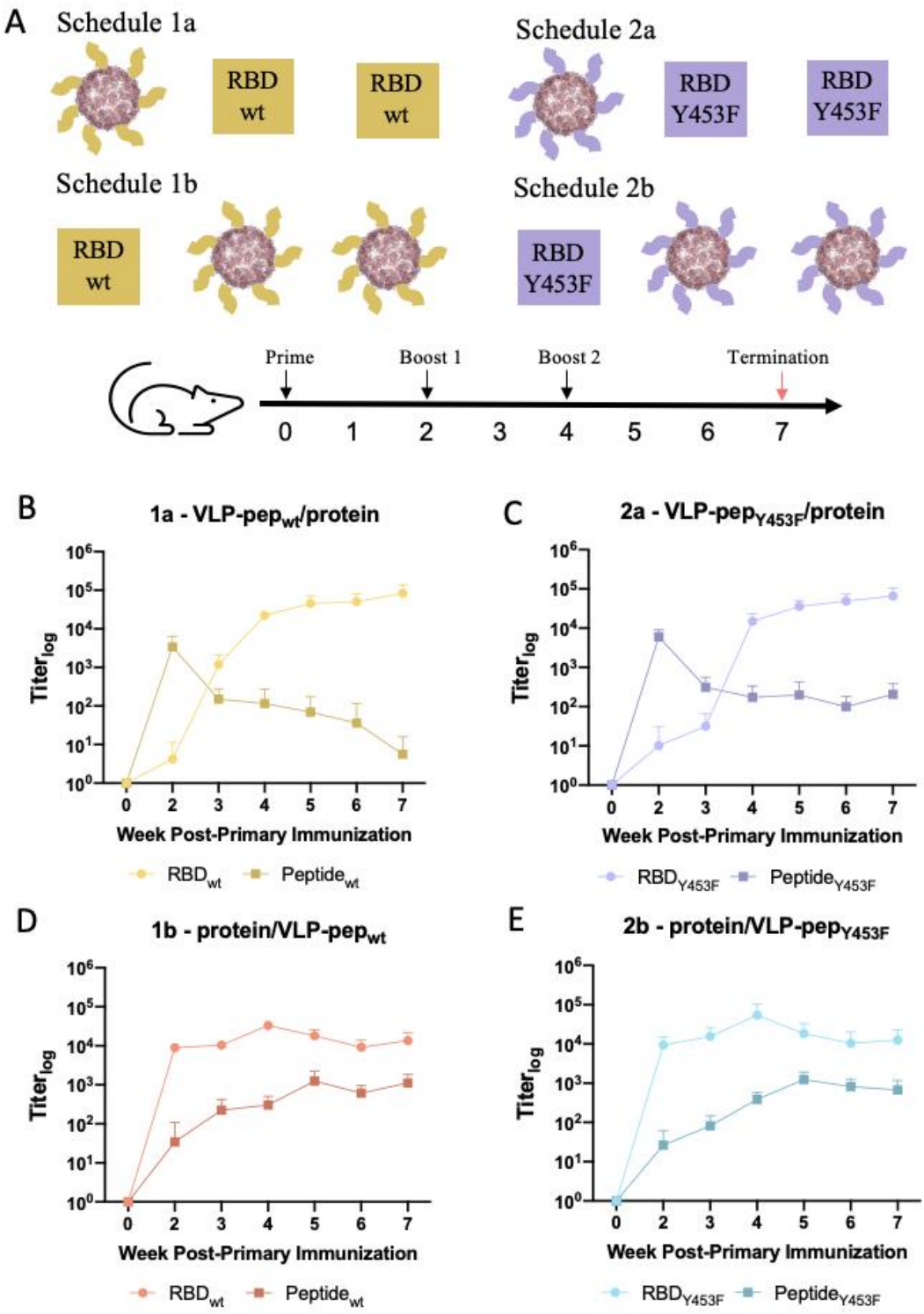

Figure 15. Immunogenicity of SARS-CoV-2 mutant peptide VLP-conjugate vaccines. (A) Immunization schedule for each of the four immunization groups each containing 5 mice. (B) Anti-RBD$_{wt}$ (yellow) and anti-peptide$_{wt}$ (dark yellow) titers over time for 1a schedule determined by ELISA. (C) Anti-RBD$_{wt}$ (red) and anti-peptide$_{wt}$ (dark red) titers over time for 1b schedule determined by ELISA. (D) Anti-RBD$_{Y453F}$ (purple) and anti-peptide$_{Y453F}$ (dark purple) titers over time for 2a schedule determined by ELISA. (E) Anti-RBD$_{Y453F}$ (blue) and anti-peptide$_{Y453F}$ (dark blue) titers over time for 2a schedule determined by ELISA.

The schedule B immunizations for both the wild type and mutant showed a far better linear peptide response over time than the schedule A immunizations (Figure 15D, 15E). They both showed a spike in anti-ecto titers at week 2 and maintained robust titers throughout. The anti-peptide response for each increased steadily to final titers at week 7 ten times less than RBD response, much greater than those seen in group A immunizations. This suggests that a far higher percentage of the humoral immune response from schedule b was directed towards the peptide of interest, increasing the probability of finding a mutant or wild type selective mAb.

At week 7 the mice with the highest antigen specific titer was from each of the vaccine groups were selected for hybridoma development. Splenectomies were performed and the B cells perfused from the spleens. The number of B cells resulting from the perfusion were within normal range for all fusions (APPENDIX B). The B cells were then electrofused with myeloma by the ImmunoDiagnostics team at the CDC to produce hybridoma.

The resultant clones were all screened for wild type and mutant RBD and peptide response by ELISA (APPENDIX B). Very few mAbs were reactive to the linear peptides and none showed reactivity to both the linear peptides and the RBD. However, just because the mAb does not bind the linear peptide does not mean it does not bind that epitope, as conformation of the peptide could play a significant role in binding ability. When analyzing solely the total number of RBD reactive clones the two immunization strategies seem to have opposite trends depending on immunization with the wild type or the mutant (Figure 16). The 1b and 2a schedules resulted in by far the highest number of mAbs reactive to both wild type and mutant RBD. This is surprising and most likely not due to any mechanistic differences between the effects of the wild type and mutant peptides.

Despite the surprising results in total number of RBD reactive mAbs, there is a clear distinction in between the A and B schedules in the results for wild type or mutant selective mAbs

(Figure 16). While the two A groups had no selective mAbs, the 1b and 2b groups had a total of 8 wild type RBD and 4 mutant RBD selective mAbs. Since the Y453F mutation removes a hydroxyl group that had the potential for an additional hydrogen bond, it follows that more mAbs would be selective for the wild type over the mutant RBD. This does make it very surprising, however, that an mAb derived from the 1B immunization which was only exposed to the wild type peptide and RBD would be selective for the mutant RBD. This result will need to be confirmed by BLI binding to each RBD. Since the goal of this experiment was to produce clones selective to one RBD over the other, the schedule in which the mice were primed with RBD and boosted with VLP-peptide was clearly more effective. This strategy suggests that the prime selects for germline B cells that bind RBD and the boost then amplifies and matures the fraction that bind the peptide of interest.

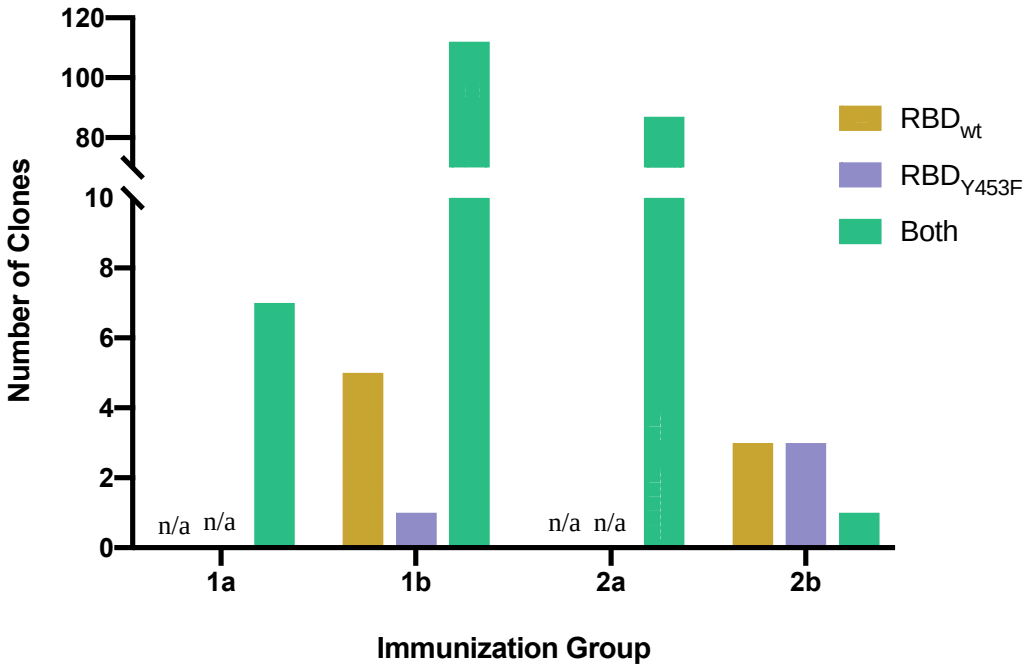

Figure 16. Binding preference of SARS-CoV-2 mutant peptide mAbs. Binding preference of mAbs from each immunization group to either wild type RBD (yellow), Y453F RBD (purple) or both (green) determined by ELISA.

5.2.5. Conclusions and Future Experimentation

These studies show that the VLP conjugate vaccine platform has the potential to be used in peptide epitope targeting. Though we do not yet have conclusive evidence to prove we successfully developed mAbs against our peptides of interest, the data shows a lot of promising early signs we did. The results from the mutant peptide experiment showed we were able direct the immune response towards the peptide of interest using a heterologous prime-boost strategy in which we primed with whole protein RBD and boosted with VLP-peptide. Using this strategy, we were able to develop mAbs with specificity towards either the wild type or Y453F mutant RBD. We were also able to produce nanomolar and sub nanomolar affinity mAbs which is important for their use as diagnostics and biological reagents.

To validate the epitope targeted by the most promising mAbs, cryo-EM structures of the mAbs binding the ectodomain are needed. This would provide conclusive evidence that were able to target specific peptides for mAb discovery. Additionally, antibody affinity is needed. To validate and build on this work we are in the process of once again trying the two different heterologous prime-boost strategies with different high-profile mutants including the K417N, E484K, and N501Y mutants relevant to which viral strains and why is this important?

5.3. α-Amanitin and Microcystin-LR Toxins

5.3.1. Toxin Structures

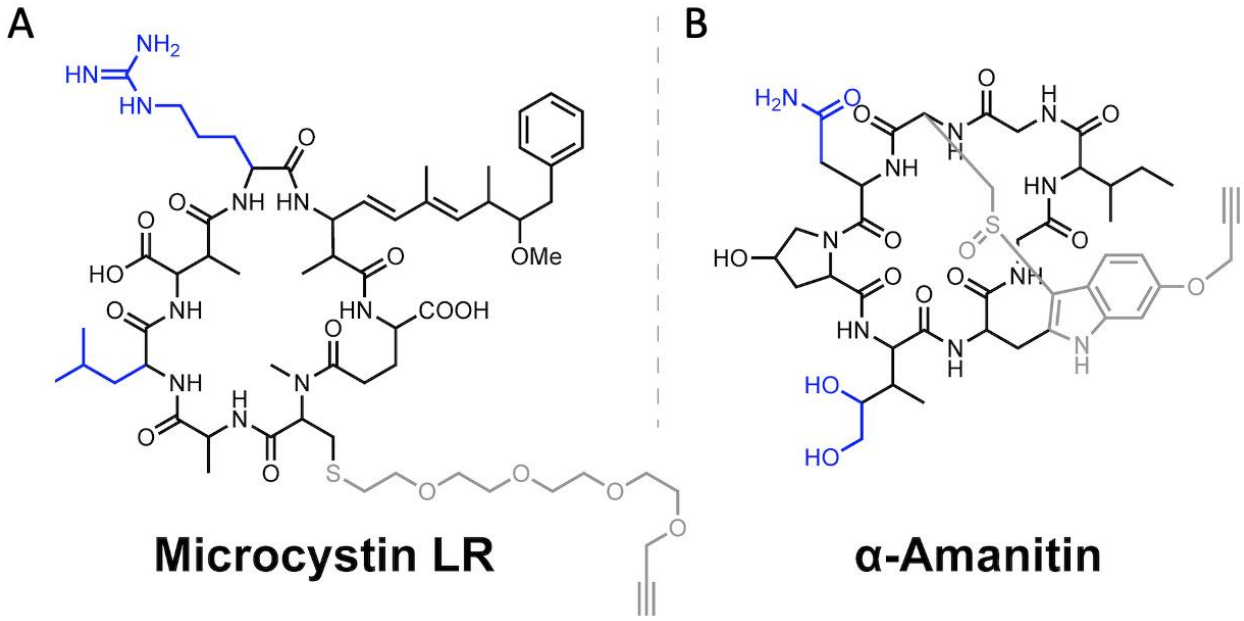

Figure 17. Structure of α-amanitin and microcystin for vaccine conjugates. The molecular structures of each toxin (blue and black) with their respective alkyne linkers (grey).

Both the microcystin LR and α-amanitin were conjugated to Qβ virus-like particles by first installing short alkyne linkers labeled in light grey (Figure 17). The functional groups labeled in blue show variable positions that distinguish each toxin from their various congeners. Microcystin LR was functionalized with a alkyne bioconjugation linkers. The lysine residues on the Qβ particles were functionalized with azide groups using NHS ester chemistry. The linker labeled toxins were then conjugated to the Qβ particles using copper-catalyzed azide-alkyne cycloaddition to create the vaccines. This allowed for multivalent display of the toxins on the surface of the VLP thereby increasing immunogenicity.

5.3.2. Toxin Immunizations

Both the microcystin LR and α-amanitin conjugate vaccines were administered at weeks 0, 2, 4 and 3 days before termination at week 8 (Figure 18A). Each immunization group consisted of four mice. The mean serum titers for each group were determined over time. The doses did turn out to be toxic to some of the mice as shown by their weights. This, however, did not seem to impact their overall immune response. The anti-microcystin LR immediately jumped to greater than 10^4 and remained there throughout the course of the immunization schedule (Figure 18B). The anti-α-amanitin titers steadily increased throughout the course of the immunization schedule to a final titer at week 8 greater than 10^4 (Figure 18C). These high titers were optimal for spleen harvest at week 8.

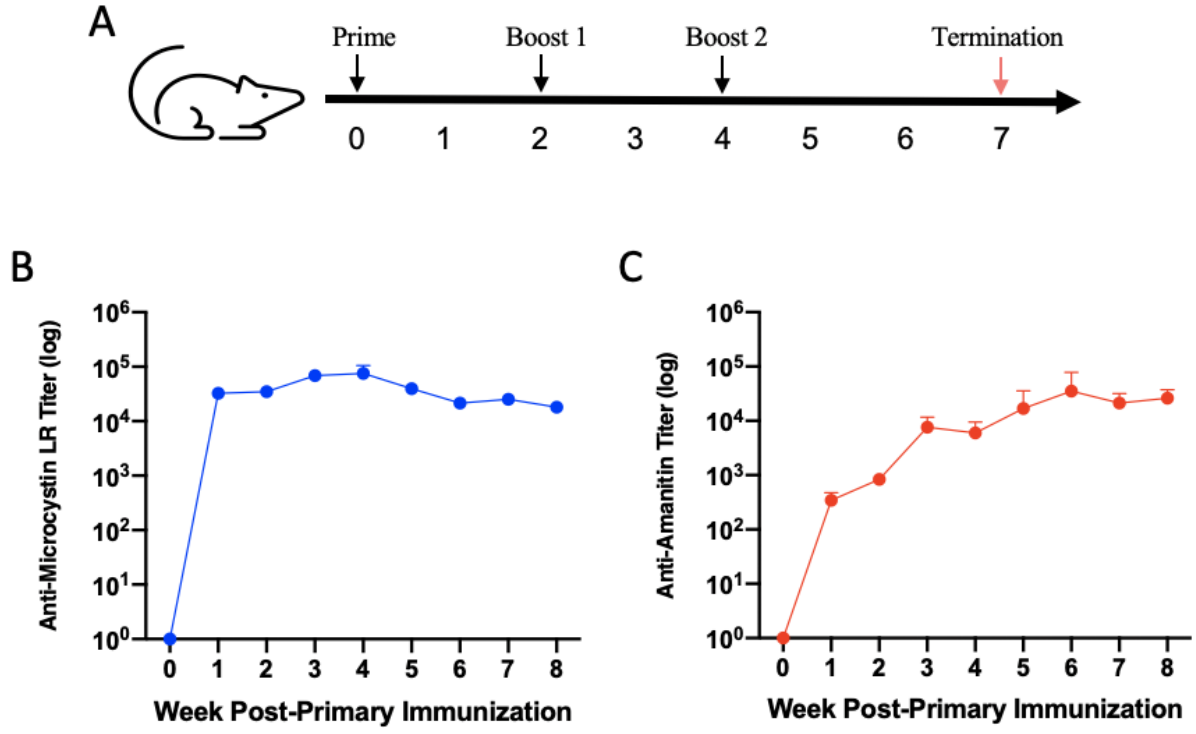

Figure 18 Immunogenicity of α-amanitin and microcystin LR VLP conjugate vaccines. (A) Immunization schedule for both α-amanitin and microcystin LR vaccines. (B) Anti-microcystin LR IgG titers over time determined by ELISA. (C) Anti-α-amanitin IgG titers over time determined by ELISA.

5.3.3. Hybridoma Fusion and Clone Characterization

At week 8 the two mice with the highest antigen specific titer was from each of the vaccine groups were selected for hybridoma development. Splenectomies were performed and the B cells perfused from the spleens. The number of B cells resulting from the perfusion were within normal range for all fusions (Figure 19).

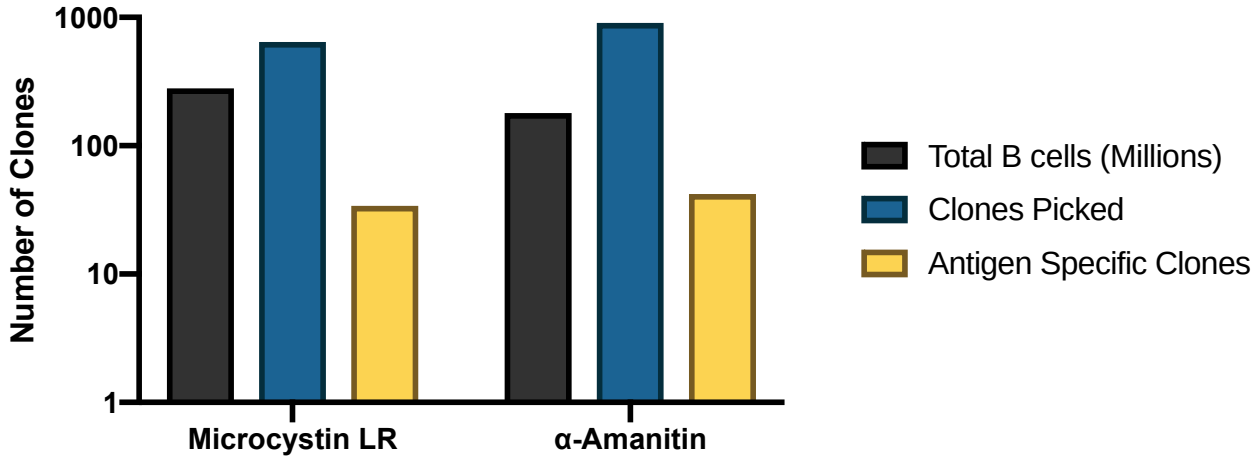

Figure 19. Statistics from α-amanitin and microcystin LR fusions. Statistics from toxin fusions with total number of B cells isolated from splenectomies (black), total number of IgG producing hybridoma picked (blue) and total number of clone lines producing cognate antigen specific mAbs (yellow) determined by ELISA.

IgG producing hybridoma were picked from each fusion and their binding ability to their cognate antigen was determined by ELISA (Figure 19). A total of 645 IgG producing clones were picked from the from the microcystin LR immunizations and 34 of these were found to bind microcystin LR. From the α-amanitin immunizations 903 clones were picked and of these 42 were positive for α-amanitin binding. The low percentage of IgG producing clones that bind to their cognate antigen in both groups is similar to those seen with the fentanyl targets and significantly lower than those seen with the peptide targets despite similar serum titers. This could be a result of fewer IGHV genetic combinations for antibody binding sites that allow for binding to small molecules.

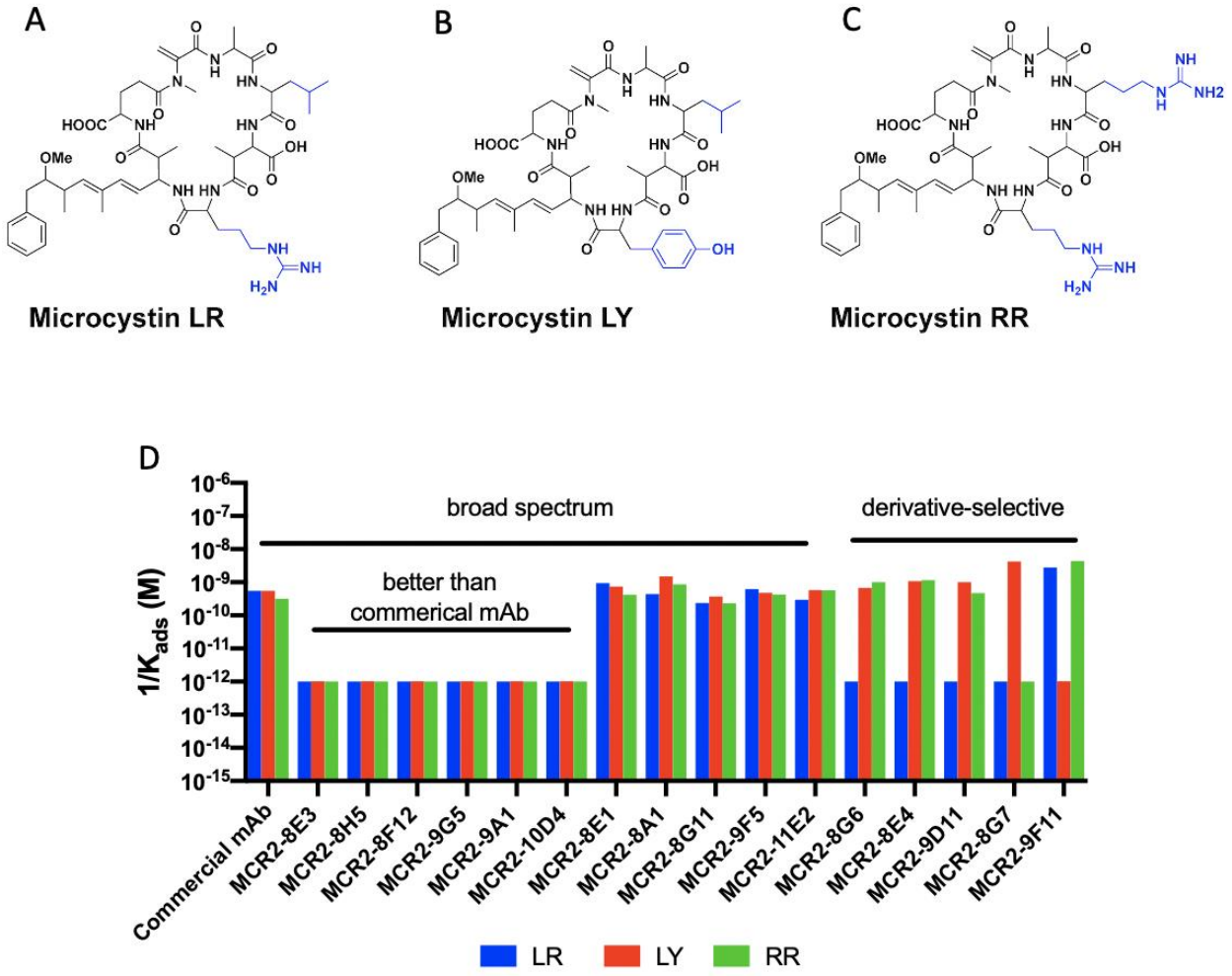

Figure 20. Analysis of microcystin LR mAbs' binding preference and affinities. (A) structure of microcystin LR. (B) structure of microcystin LY. (C) structure of microcystin RR. (D) Binding affinities shown as $1/K_{ads}$ of 16 mAbs derived from microcystin LR immunizations for all three microcystin variants. Binding affinities determined by BLI.

There are three commonly found microcystin variants that have the potential to contaminate water supplies microcystin LR, microcystin LY, and microcystin RR (Figure 20A, B, C). Overall, the structures are very similar aside from functional group changes in two locations labeled in blue, making broad spectrum mAbs far more easily attainable than derivative selective clones. BLI was performed by CDC on each of the microcystin LR immunization derived mAbs to test for binding affinity to each variant (Figure 20B). A commercially available mAb was also analyzed for comparison. The commercial mAb had broad spectrum sub nanomolar binding

affinity. We were able to isolate six broad spectrum clones (MRC2-8E3, MRC2-8H5, MRC2-8F12, MRC2-9G5, MRC2-9A1, and MRC2-10D4) with sub picomolar binding affinities. Since they bind each variant with an equal affinity, their most important binding epitopes probably rely on the conserved regions between each of the molecules. The better binding affinity of these clones means they could be used to create a more sensitive diagnostic field test.

We also isolated three mAbs (MRC2-8G6, MRC2-8E4, and MRC2-9D11) that bind microcystin LR with a higher affinity than microcystin LY or microcystin RR. This indicates that both the isobutyl and guanidino groups on microcystin LR play an important role in binding for each mAb that the substitutions on microcystin LY or microcystin RR interfere with. One mAb (MRC2-8G7) had a higher affinity for both microcystin LR and microcystin RR than microcystin LY. This most likely indicates that the guanidino group on microcystin LR and microcystin RR plays an important role in MRC2-8G7 mAb binding that the substitution on microcystin LY interferes with. One mAb (MCR2-9F11) had a higher affinity for microcystin LY than microcystin LR and microcystin RR. This indicates that both the isobutyl and phenol groups on microcystin LY play an important role in MCR2-9F11 binding the substitutions on microcystin LR and microcystin RR interferes with. These derivative selective mAbs could be used to help in diagnostic differentiation between the three derivatives.

5.3.4. Conclusions and Future Experimentation

In this study, we were able to successfully create an immune response against toxins microcystin LR and α-amanitin using a VLP conjugate vaccine platform. We were able to generate robust antigen-specific IgG titers for both constructs. We were able to isolate 34 clones producing mAbs that were reactive to microcystin LR and 42 clones producing mAbs that were reactive to

α-amanitin. Of the clones that bound microcystin LR we were able to identify six with sub picomolar dissociation constants for all three microcystin variants which is orders of magnitude higher affinity than the current commercially available mAbs. We were also able to identify three mAbs with microcystin LR selectivity, one mAb with microcystin LR and microcystin RR selectivity, and one mAb with microcystin LY selectivity. There derivative selective mAbs have the potential to be used in diagnostics for variant differentiation. The next steps in this work will include sequencing of all the high affinity broad spectrum and derivative-selective mAbs. With this data we can determine if some of these mAbs with similar binding patterns and affinities also have similar antibody binding sequences, helping us to make more mechanistic conclusions.

CONCLUSIONS

This thesis displays the potential for VLP conjugate vaccines to be used with a variety of immunization strategies in order to create mouse humoral immune responses against an array of target molecules ideal for mAb development. First, we were able to create an optimized immunization strategy using PBS-57, an NKT agonist adjuvant, and VLP-fentanyl vaccines to produce high IgG titers against eight fentanyl derivatives. We then used the B cells derived from these immunizations to produce hybridoma clonal cell lines capable of producing mAbs with 14 unique binding patterns to these fentanyl derivatives. One of these mAbs was even capable of selectively binding only the acetyl αMe-fentanyl derivative. We then showed that 6 of these mAbs could be used in a diagnostic test to positively differentiate between each derivative. Lastly, we proved that these mAbs did not have any significant interaction with naloxone, meaning they could be used in a two-step combined treatment plan. These mAbs have the potential to be used as reagents, diagnostics, and therapeutics to help the current fentanyl epidemic in the United States. These results also confirm that mAbs can be derived from the robust IgG immune response elicited by hapten conjugate VLP vaccines.

Next, we used this method to develop mAbs for specific SARS-CoV-2 peptide targets. We were able to direct a polyclonal immune response towards certain epitopes using linear peptide display on the VLP while maintaining conformational specificity by using a heterologous prime-boost strategy. We determined that the optimal sequence is to prime with whole protein RBD and boost with VLP-peptide. Using this strategy, we were able to isolate 8 mAbs that selectively bind the wild type RBD and 4 that selectively bind the Y453F mutant RBD. The mAbs that resulted from the neutralizing peptides are currently in use at CDC as reagents in biological assays, helping with research for the current COVID-19 epidemic. These results also suggest that peptide

conjugate VLP vaccines in conjunction with whole protein immunizations can be used to create peptide specific and conformationally accurate mAbs.

Lastly, we used this method to develop high-affinity mAbs for the toxins α-amanitin and microcystin LR. Using conjugate Qβ vaccines we were able to produce high IgG titers against each of the toxins. Using B cells derived from these immunizations, we were able to isolate 34 microcystin LR reactive hybridoma clonal cell lines and 42 α-amanitin reactive clonal cell lines. Of the microcystin LR mAbs we were able to find six with a higher affinity for all three microcystin variants than the commercially available mAbs. Additionally, we were able to identify three mAbs with microcystin LR selectivity, one mAb with microcystin LR and microcystin RR selectivity, and one mAb with microcystin LY selectivity. These mAbs can be used as broad spectrum or differentiating diagnostics for contamination with α-amanitin or the three microcystin variants. These results also confirm the ability of conjugate VLP vaccines to increase the immunogenicity while decreasing the toxicity of cyclic peptides.

Combined this data displays the versatility of the VLP vaccine platform in eliciting robust IgG immune responses against an array of targets. The success in developing mAbs using hybridoma technology from these VLP immunizations shows the conjugate VLP platform's potential as an initial means of immunization with the ultimate goal of mAb development.

REFERENCES

1. Siddiqui, M., Monoclonal antibodies as diagnostics; an appraisal. *Indian journal of pharmaceutical sciences* **2010,** *72* (1), 12.
2. Waldmann, T. A., Immunotherapy: past, present and future. *Nat. Med.* **2003,** *9* (3), 269-277.
3. Corti, A.; Piro, P.; Carta, E.; Rovelli, C.; Bassi, R.; Lamponi, S.; Morgese, N.; Rurali, C.; Tognella, S., Device and method for pregnancy detection. Google Patents: 1992.
4. Mahmuda, A.; Bande, F.; Al-Zihiry, K. J. K.; Abdulhaleem, N.; Majid, R. A.; Hamat, R. A.; Abdullah, W. O.; Unyah, Z., Monoclonal antibodies: A review of therapeutic applications and future prospects. *Tropical Journal of Pharmaceutical Research* **2017,** *16* (3), 713-722.
5. Bachmann, M. F.; Jennings, G. T., Vaccine delivery: a matter of size, geometry, kinetics and molecular patterns. *Nature Reviews Immunology* **2010,** *10* (11), 787-796.
6. Murphy, K.; Weaver, C., *Janeway's immunobiology*. Garland Science: 2016.
7. Cresswell, P., Assembly, transport, and function of MHC class II molecules. *Annu. Rev. Immunol.* **1994,** *12* (1), 259-291.
8. Manolova, V.; Flace, A.; Bauer, M.; Schwarz, K.; Saudan, P.; Bachmann, M. F., Nanoparticles target distinct dendritic cell populations according to their size. *Eur. J. Immunol.* **2008,** *38* (5), 1404-1413.
9. Spencer, M.; Warner, M.; Bastian, B. A.; Trinidad, J. P.; Hedegaard, H., Drug overdose deaths involving fentanyl. **2019**.
10. COVID-19 Dashboard. https://coronavirus.jhu.edu/map.html.
11. Filigenzi, M. S.; Poppenga, R. H.; Tiwary, A. K.; Puschner, B., Determination of α-amanitin in serum and liver by multistage linear ion trap mass spectrometry. *Journal of agricultural and food chemistry* **2007,** *55* (8), 2784-2790.
12. Rantala, A.; Rajaniemi-Wacklin, P.; Lyra, C.; Lepistö, L.; Rintala, J.; Mankiewicz-Boczek, J.; Sivonen, K., Detection of microcystin-producing cyanobacteria in Finnish lakes with genus-specific microcystin synthetase gene E (mcyE) PCR and associations with environmental factors. *Appl. Environ. Microbiol.* **2006,** *72* (9), 6101-6110.
13. Köhler, G.; Milstein, C., Continuous cultures of fused cells secreting antibody of predefined specificity. *Nature* **1975,** *256* (5517), 495-497.
14. Gómez-Hens, A.; Fernández-Romero, J.; Aguilar-Caballos, M., Nanostructures as analytical tools in bioassays. *TrAC, Trends Anal. Chem.* **2008,** *27* (5), 394-406.
15. Hooks, M. A.; Wade, C. S.; Millikan Jr, W. J., Muromonab CD-3: a review of its pharmacology, pharmacokinetics, and clinical use in transplantation. *Pharmacotherapy: The Journal of Human Pharmacology and Drug Therapy* **1991,** *11* (1), 26-37.
16. Cai, H. H., Therapeutic Monoclonal Antibodies Approved by FDA in 2020. **2021**.
17. Shoae, M.; Khorashadizadeh, M.; Derakhshani, A.; Safarnejad, M. R.; Safarpour, H., An overview of the current status of engineered therapeutic monoclonal antibodies. *International Pharmacy Acta* **2019,** *2* (1), 2-9: 1-10.
18. Pandey, S., Hybridoma technology for production of monoclonal antibodies. *Hybridoma* **2010,** *1* (2), 017.
19. Chackerian, B., Virus-like particles: flexible platforms for vaccine development. *Expert review of vaccines* **2007,** *6* (3), 381-390.

20. Polonskaya, Z.; Deng, S.; Sarkar, A.; Kain, L.; Comellas-Aragones, M.; McKay, C. S.; Kaczanowska, K.; Holt, M.; McBride, R.; Palomo, V., T cells control the generation of nanomolar-affinity anti-glycan antibodies. *The Journal of clinical investigation* **2017,** *127* (4), 1491-1504.
21. van den Worm, S. H.; Koning, R. I.; Warmenhoven, H. J.; Koerten, H. K.; van Duin, J., Cryo electron microscopy reconstructions of the Leviviridae unveil the densest icosahedral RNA packing possible. *J. Mol. Biol.* **2006,** *363* (4), 858-865.
22. Tars, K.; Fridborg, K.; Bundule, M.; Liljas, L., Structure determination of bacteriophage PP7 from Pseudomonas aeruginosa: from poor data to a good map. *Acta Crystallogr. Sect. D: Biol. Crystallogr.* **2000,** *56* (4), 398-405.
23. Golmohammadi, R.; Fridborg, K.; Bundule, M.; Valegård, K.; Liljas, L., The crystal structure of bacteriophage Qβ at 3.5 Å resolution. *Structure* **1996,** *4* (5), 543-554.
24. Fiedler, J. D.; Higginson, C.; Hovlid, M. L.; Kislukhin, A. A.; Castillejos, A.; Manzenrieder, F.; Campbell, M. G.; Voss, N. R.; Potter, C. S.; Carragher, B., Engineered mutations change the structure and stability of a virus-like particle. *Biomacromolecules* **2012,** *13* (8), 2339-2348.
25. Caldeira, J. C.; Peabody, D. S., Stability and assembly in vitro of bacteriophage PP7 virus-like particles. *Journal of nanobiotechnology* **2007,** *5* (1), 10.
26. Zhao, L.; Kopylov, M.; Potter, C. S.; Carragher, B.; Finn, M., Engineering the PP7 virus capsid as a peptide display platform. *ACS nano* **2019,** *13* (4), 4443-4454.
27. Pokorski, J. K.; Hovlid, M. L.; Finn, M., Cell targeting with hybrid Qβ virus-like particles displaying epidermal growth factor. *ChemBioChem* **2011,** *12* (16), 2441-2447.
28. Cox, J. C.; Coulter, A. R., Adjuvants—a classification and review of their modes of action. *Vaccine* **1997,** *15* (3), 248-256.
29. Jennings, V. M., Review of selected adjuvants used in antibody production. *ILAR journal* **1995,** *37* (3), 119-125.
30. Waksman, B. H. In *Adjuvants and immune regulation by lymphoid cells*, Springer Semin. Immunopathol., Springer: 1979; pp 5-33.
31. Fujii, S.; Motohashi, S.; Shimizu, K.; Nakayama, T.; Yoshiga, Y.; Taniguchi, M. In *Adjuvant activity mediated by iNKT cells*, Semin. Immunol., Elsevier: 2010; pp 97-102.
32. Koch, M.; Stronge, V. S.; Shepherd, D.; Gadola, S. D.; Mathew, B.; Ritter, G.; Fersht, A. R.; Besra, G. S.; Schmidt, R. R.; Jones, E. Y., The crystal structure of human CD1d with and without α-galactosylceramide. *Nat. Immunol.* **2005,** *6* (8), 819-826.
33. Chapman, A. P.; Tang, X.; Lee, J. R.; Chida, A.; Mercer, K.; Wharton, R. E.; Kainulainen, M. H.; Harcourt, J. L.; Martines, R. B.; Schroeder, M.; Zhao, L.; Bryksin, A.; Zhou, B.; Bergeron, E.; Bollweg, B. C.; Tamin, A.; Thornburg, N.; Wentworth, D. E.; Petway, D.; Bagarozzi, D.; Finn, M. G.; Goldstein, J. M., Rapid Development of Neutralizing and Diagnostic SARS-COV-2 Mouse Monoclonal Antibodies. *BioRxiv* **2020**.
34. Armenian, P.; Vo, K. T.; Barr-Walker, J.; Lynch, K. L., Fentanyl, fentanyl analogs and novel synthetic opioids: a comprehensive review. *Neuropharmacology* **2018,** *134*, 121-132.
35. Van Bever, W. F.; Niemegeers, C. J.; Janssen, P. A., Synthetic analgesics. Synthesis and pharmacology of the diastereoisomers of N-[3-methyl-1-(2-phenylethyl)-4-piperidyl]-N-phenylpropanamide and N-[3-methyl-1-(1-methyl-2-phenylethyl)-4-piperidyl]-N-phenylpropanamide. *Journal of medicinal chemistry* **1974,** *17* (10), 1047-1051.

36. Jones, C. M.; Einstein, E. B.; Compton, W. M., Changes in synthetic opioid involvement in drug overdose deaths in the United States, 2010-2016. *Jama* **2018,** *319* (17), 1819-1821.
37. Krenzelok, E. P., Abuse of fentanyl derivatives: History repeating itself. *American Journal of Health-System Pharmacy* **2017,** *74* (8), 556-556.
38. Amlani, A.; McKee, G.; Khamis, N.; Raghukumar, G.; Tsang, E.; Buxton, J. A., Why the FUSS (Fentanyl Urine Screen Study)? A cross-sectional survey to characterize an emerging threat to people who use drugs in British Columbia, Canada. *Harm reduction journal* **2015,** *12* (1), 54.
39. Arfken, C. L.; Suchanek, J.; Greenwald, M. K., Characterizing fentanyl use in methadone-maintained clients. *J. Subst. Abuse Treat.* **2017,** *75*, 17-21.
40. Niemegeers, C.; Janssen, P., Alfentanil (R 39 209)—a particularly short-acting intravenous narcotic analgesic in rats. *Drug Development Research* **1981,** *1* (1), 83-88.
41. Townsend, E. A.; Bremer, P. T.; Faunce, K. E.; Negus, S. S.; Jaster, A. M.; Robinson, H. L.; Janda, K. D.; Banks, M. L., Evaluation of a dual fentanyl/heroin vaccine on the antinociceptive and reinforcing effects of a fentanyl/heroin mixture in male and female rats. *ACS chemical neuroscience* **2020,** *11* (9), 1300-1310.
42. Jackson, H., The evaluation of analgesic potency of drugs using thermal stimulation in the rat. *British journal of pharmacology and chemotherapy* **1952,** *7* (2), 196.
43. Chen, Q.; Shang, Y.; Xu, Y.; Li, P.; Liu, G.-L., Analgesic effect and pharmacological mechanism of fentanyl and butorphanol in a rat model of incisional pain. *Journal of clinical anesthesia* **2016,** *28*, 67-73.
44. Addiction, E. M. C. f. D. a. D., Report on the risk assessment of methyl 1-(2-phenylethyl)-4-[phenyl(propanoyl)amino]piperidine-4-carboxylate (carfentanil) in the framework of the Counsil Decision on new psychoactive substances. Luxembourg, 2018.
45. Mather, L., Clinical pharmacokinetics of fentanyl and its newer derivatives. *Clin. Pharmacokin.* **1983,** *8* (5), 422-446.
46. Sawynok, J., The therapeutic use of heroin: a review of the pharmacological literature. *Can. J. Physiol. Pharmacol.* **1986,** *64* (1), 1-6.
47. Ngai, S.; Berkowitz, B. A.; Yang, J.; Hempstead, J.; Spector, S., Pharmacokinetics of naloxone in rats and in man: basis for its potency and short duration of action. *Anesthesiology* **1976,** *44* (5), 398-401.
48. Smith, L. C.; Bremer, P. T.; Hwang, C. S.; Zhou, B.; Ellis, B.; Hixon, M. S.; Janda, K. D., Monoclonal antibodies for combating synthetic opioid intoxication. *J. Am. Chem. Soc.* **2019,** *141* (26), 10489-10503.
49. Masters, P. S., The molecular biology of coronaviruses. *Advances in virus research* **2006,** *66*, 193-292.
50. Cucinotta, D.; Vanelli, M., WHO declares COVID-19 a pandemic. *Acta Bio Medica: Atenei Parmensis* **2020,** *91* (1), 157.
51. Shang, J.; Wan, Y.; Luo, C.; Ye, G.; Geng, Q.; Auerbach, A.; Li, F., Cell entry mechanisms of SARS-CoV-2. *Proc. Natl. Acad. Sci. USA* **2020,** *117* (21), 11727-11734.
52. Shang, J.; Ye, G.; Shi, K.; Wan, Y.; Luo, C.; Aihara, H.; Geng, Q.; Auerbach, A.; Li, F., Structural basis of receptor recognition by SARS-CoV-2. *Nature* **2020,** *581* (7807), 221-224.

53. Ju, B.; Zhang, Q.; Ge, J.; Wang, R.; Sun, J.; Ge, X.; Yu, J.; Shan, S.; Zhou, B.; Song, S., Human neutralizing antibodies elicited by SARS-CoV-2 infection. *Nature* **2020,** *584* (7819), 115-119.
54. Shi, R.; Shan, C.; Duan, X.; Chen, Z.; Liu, P.; Song, J.; Song, T.; Bi, X.; Han, C.; Wu, L., A human neutralizing antibody targets the receptor-binding site of SARS-CoV-2. *Nature* **2020,** *584* (7819), 120-124.
55. Liu, L.; Wang, P.; Nair, M. S.; Yu, J.; Rapp, M.; Wang, Q.; Luo, Y.; Chan, J. F.-W.; Sahi, V.; Figueroa, A., Potent neutralizing antibodies against multiple epitopes on SARS-CoV-2 spike. *Nature* **2020,** *584* (7821), 450-456.
56. Chi, X.; Yan, R.; Zhang, J.; Zhang, G.; Zhang, Y.; Hao, M.; Zhang, Z.; Fan, P.; Dong, Y.; Yang, Y., A neutralizing human antibody binds to the N-terminal domain of the Spike protein of SARS-CoV-2. *Science* **2020,** *369* (6504), 650-655.
57. Zhou, P.; Shi, Z.-L., SARS-CoV-2 spillover events. *Science* **2021,** *371* (6525), 120-122.
58. Lan, J.; Ge, J.; Yu, J.; Shan, S.; Zhou, H.; Fan, S.; Zhang, Q.; Shi, X.; Wang, Q.; Zhang, L., Structure of the SARS-CoV-2 spike receptor-binding domain bound to the ACE2 receptor. *Nature* **2020,** *581* (7807), 215-220.
59. Koopmans, M., SARS-CoV-2 and the human-animal interface: outbreaks on mink farms. *The Lancet Infectious Diseases* **2021,** *21* (1), 18-19.
60. Hayashi, T.; Yaegashi, N.; Konishi, I., Effect of RBD mutation (Y453F) in spike glycoprotein of SARS-CoV-2 on neutralizing antibody affinity. *BioRxiv* **2020**.
61. Hoffmann, M.; Zhang, L.; Krüger, N.; Graichen, L.; Kleine-Weber, H.; Hofmann-Winkler, H.; Kempf, A.; Nessler, S.; Riggert, J.; Winkler, M. S., SARS-CoV-2 mutations acquired in mink reduce antibody-mediated neutralization. *BioRxiv* **2021**.
62. Santi, L.; Maggioli, C.; Mastroroberto, M.; Tufoni, M.; Napoli, L.; Caraceni, P., Acute liver failure caused by Amanita phalloides poisoning. *International journal of hepatology* **2012,** *2012*.
63. McLellan, N. L.; Manderville, R. A., Toxic mechanisms of microcystins in mammals. *Toxicology research* **2017,** *6* (4), 391-405.
64. Wharton, R. E.; Casbohm, J.; Hoffmaster, R.; Brewer, B. N.; Finn, M.; Johnson, R. C., Detection of 30 Fentanyl Analogs by Commercial Immunoassay Kits. *J. Anal. Toxicol.* **2021**.
65. Laudenbach, M.; Tucker, A.; Runyon, S.; Carroll, F.; Pravetoni, M., The frequency of early-activated hapten-specific B cell subsets predicts the efficacy of vaccines for nicotine dependence. *Vaccine* **2015,** *33* (46), 6332-6339.
66. Orson, F. M.; Rossen, R. D.; Shen, X.; Lopez, A. Y.; Wu, Y.; Kosten, T. R., Spontaneous development of IgM anti-cocaine antibodies in habitual cocaine users: effect on IgG antibody responses to a cocaine cholera toxin B conjugate vaccine. *The American journal on addictions* **2013,** *22* (2), 169-174.
67. Liu, Z.; Guo, J., NKT-cell glycolipid agonist as adjuvant in synthetic vaccine. *Carbohydr. Res.* **2017,** *452*, 78-90.
68. Jones, M.; Hay, F., The isotype and specificity of antiglobulins in BALB/c mice. *Clinical and experimental immunology* **1985,** *59* (2), 475.
69. Collins, A. M., IgG subclass co-expression brings harmony to the quartet model of murine IgG function. *Immunol. Cell Biol.* **2016,** *94* (10), 949-954.

70. Turner, M. L.; Corcoran, L. M.; Brink, R.; Hodgkin, P. D., High-affinity B cell receptor ligation by cognate antigen induces cytokine-independent isotype switching. *The Journal of Immunology* **2010,** *184* (12), 6592-6599.
71. Collins, A. M.; Wang, Y.; Roskin, K. M.; Marquis, C. P.; Jackson, K. J., The mouse antibody heavy chain repertoire is germline-focused and highly variable between inbred strains. *Philos. Trans. R. Soc. London, Ser. B* **2015,** *370* (1676), 20140236.
72. Cai, Y.; Zhang, J.; Xiao, T.; Peng, H.; Sterling, S. M.; Walsh, R. M.; Rawson, S.; Rits-Volloch, S.; Chen, B., Distinct conformational states of SARS-CoV-2 spike protein. *Science* **2020,** *369* (6511), 1586-1592.

APPENDIX

APPENDIX A: PP7-wt fentanyl conjugate vaccines

DLS of PP7-Fentanyl Conjugate Vaccines

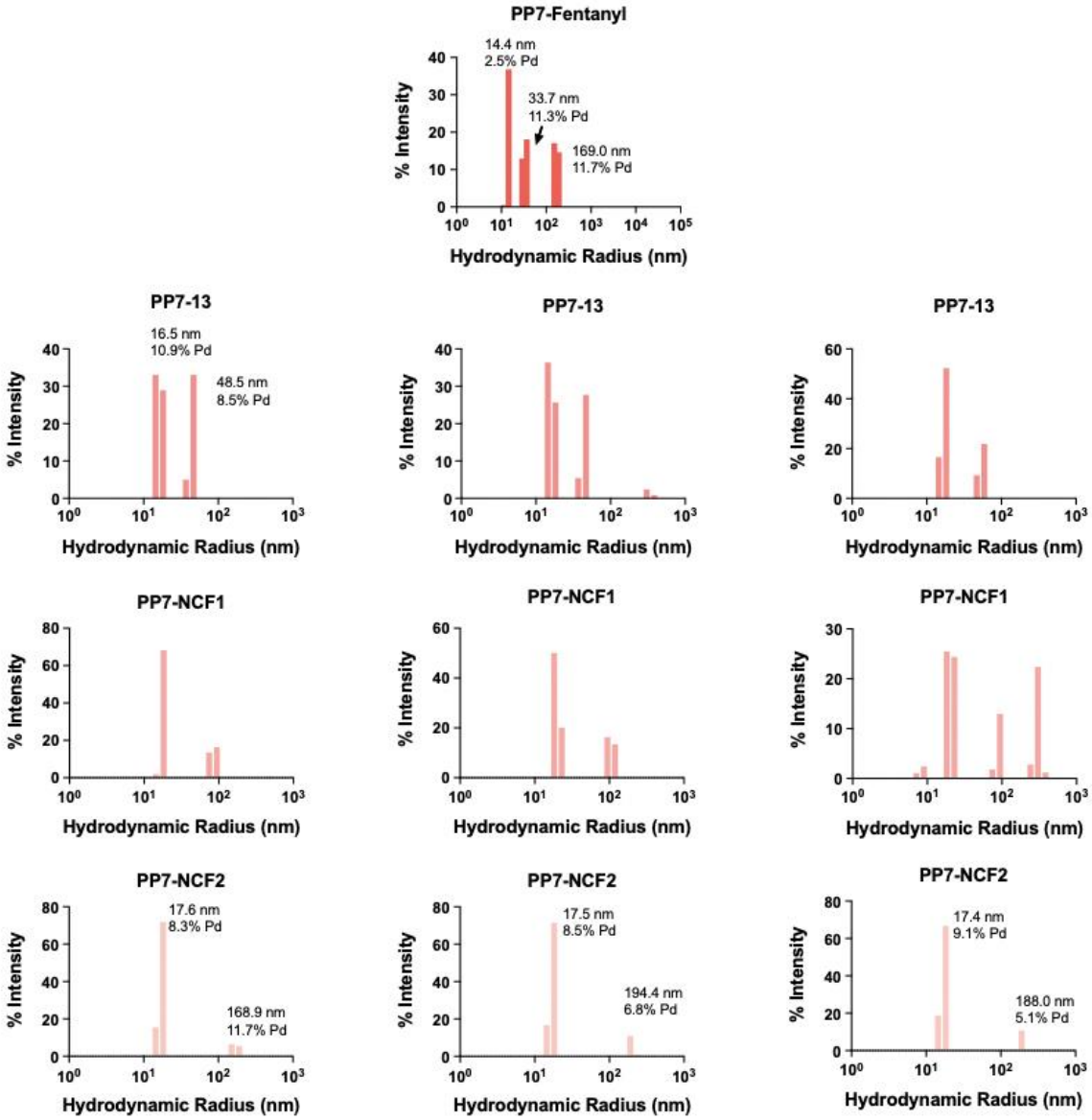

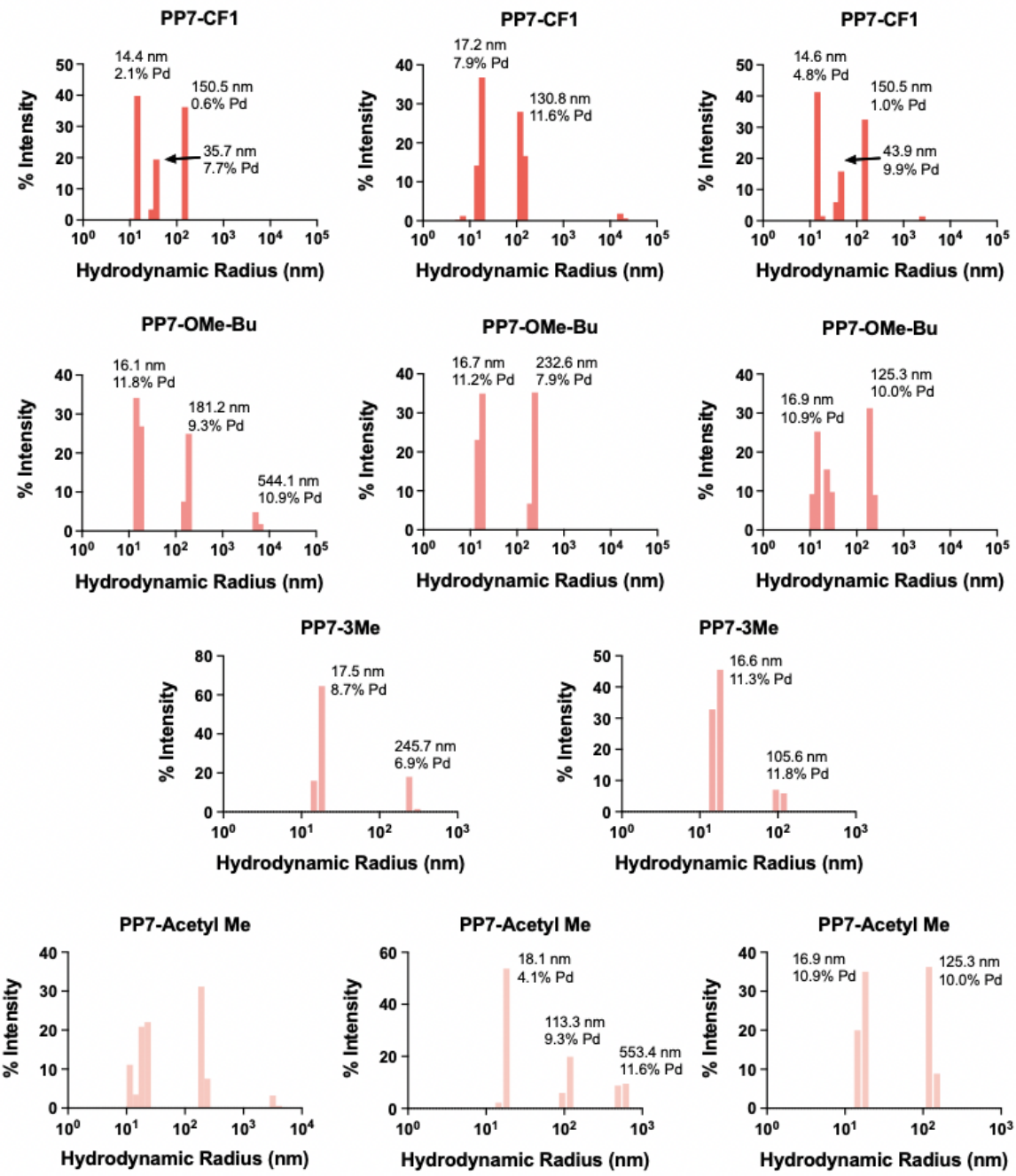
PP7-CF1
14.4 nm
2.1% Pd
150.5 nm
0.6% Pd
35.7 nm
7.7% Pd
% Intensity
Hydrodynamic Radius (nm)
PP7-CF1
17.2 nm
7.9% Pd
130.8 nm
11.6% Pd
% Intensity
Hydrodynamic Radius (nm)
PP7-CF1
14.6 nm
4.8% Pd
150.5 nm
1.0% Pd
43.9 nm
9.9% Pd
% Intensity
Hydrodynamic Radius (nm)
PP7-OMe-Bu
16.1 nm
11.8% Pd
181.2 nm
9.3% Pd
544.1 nm
10.9% Pd
% Intensity
Hydrodynamic Radius (nm)
PP7-OMe-Bu
16.7 nm
11.2% Pd
232.6 nm
7.9% Pd
% Intensity
Hydrodynamic Radius (nm)
PP7-OMe-Bu
16.9 nm
10.9% Pd
125.3 nm
10.0% Pd
% Intensity
Hydrodynamic Radius (nm)
PP7-3Me
17.5 nm
8.7% Pd
245.7 nm
6.9% Pd
% Intensity
Hydrodynamic Radius (nm)
PP7-3Me
16.6 nm
11.3% Pd
105.6 nm
11.8% Pd
% Intensity
Hydrodynamic Radius (nm)
PP7-Acetyl Me
% Intensity
Hydrodynamic Radius (nm)
PP7-Acetyl Me
18.1 nm
4.1% Pd
113.3 nm
9.3% Pd
553.4 nm
11.6% Pd
% Intensity
Hydrodynamic Radius (nm)
PP7-Acetyl Me
16.9 nm
10.9% Pd
125.3 nm
10.0% Pd
% Intensity
Hydrodynamic Radius (nm)

FPLC of PP7-Fentanyl Conjugate Vaccines.

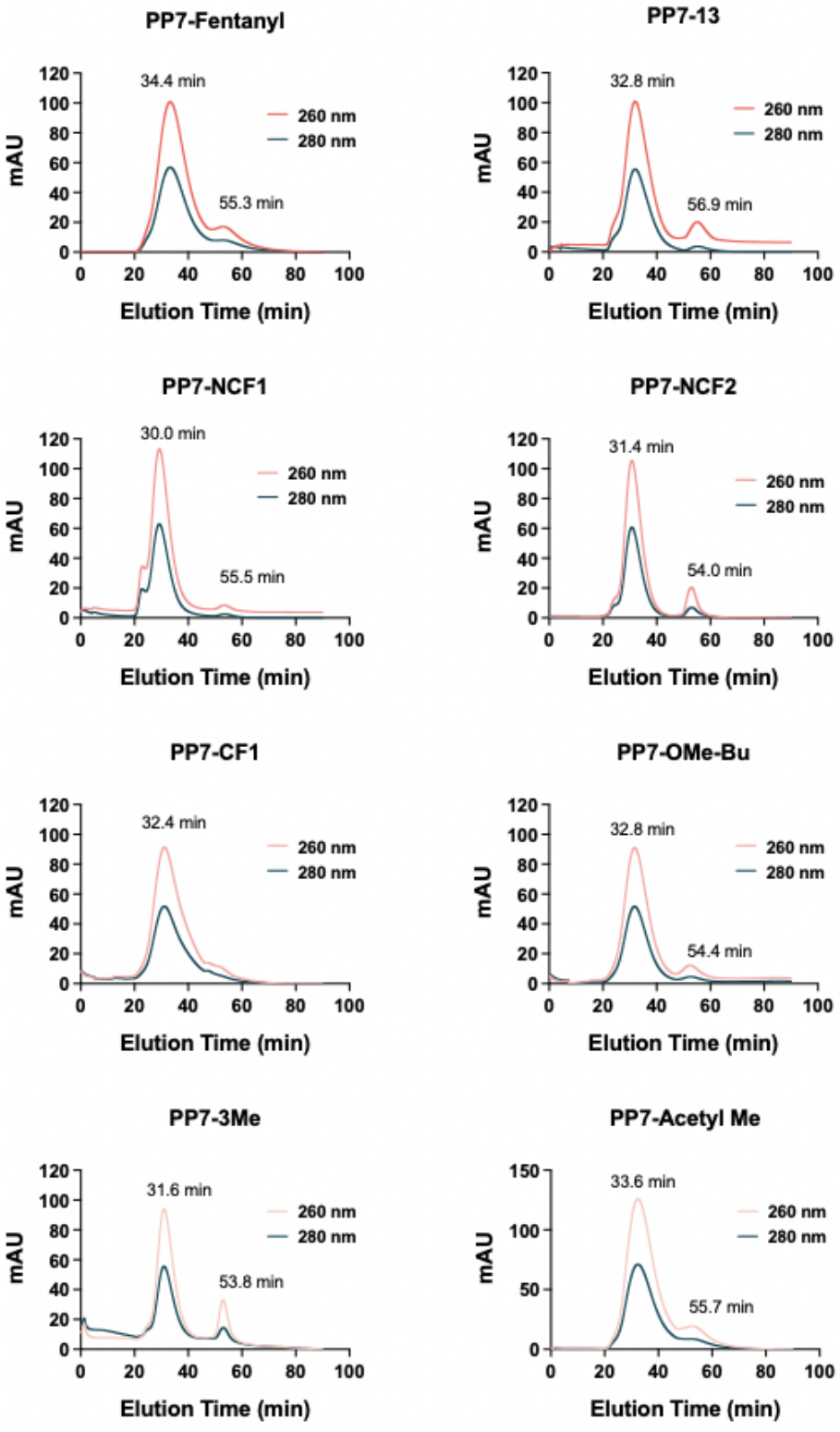

LCMS of PP7-Fentanyl Conjugate Vaccines.

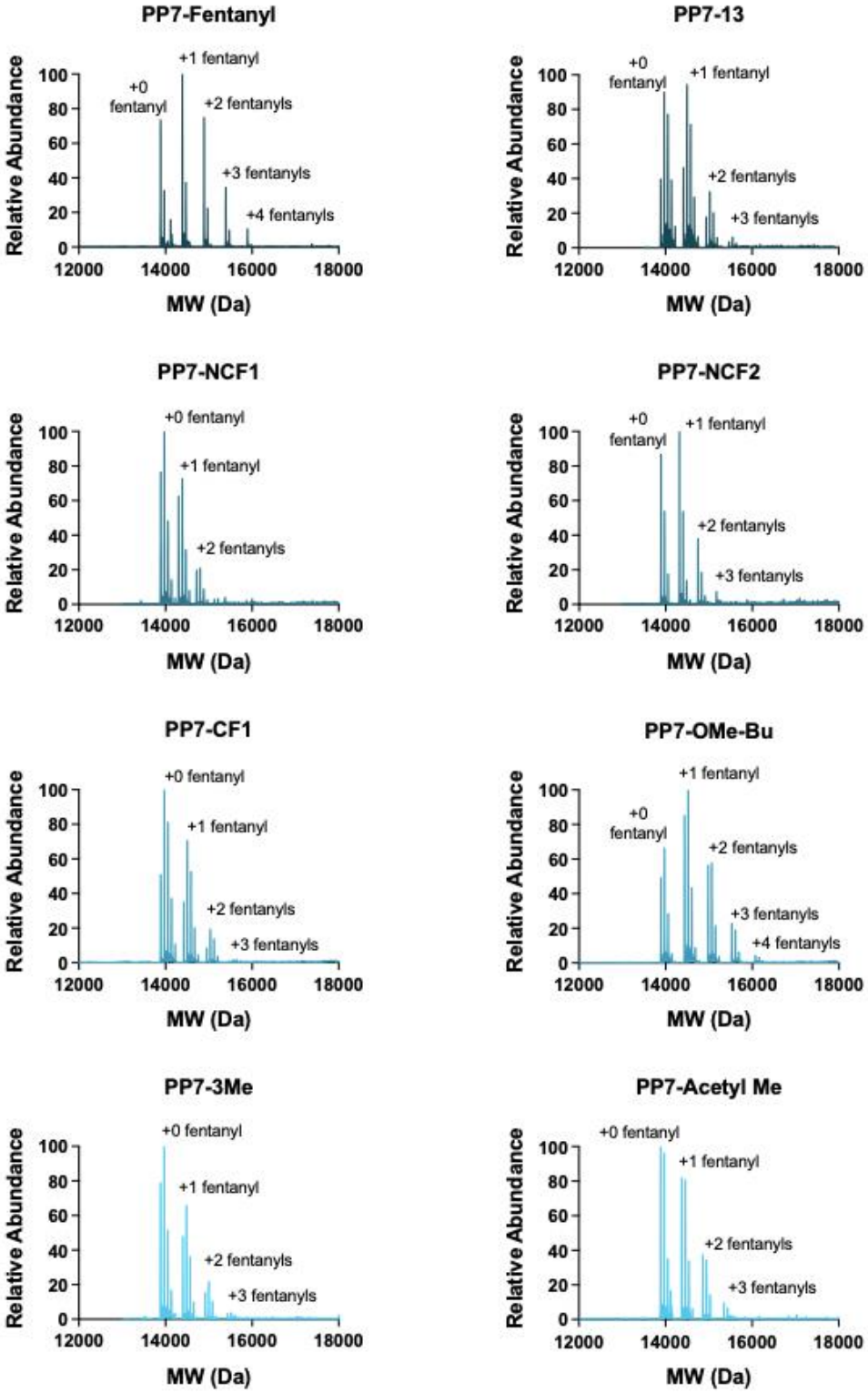

Chemical Modification of PP7-Fentanyl Conjugate Vaccines

Vaccine Fentanyl (all PP7 VLP)	Fentanyl Class	# linkers/VLP	# Fentanyls/ VLP	Fentanyl Dose (mg/kg)
Fentanyl	0	274	228	0.1
Furanyl Benzyl Fentanyl (13)	n/a	431	135	0.06
Norcarfentanil-1 (NCF1)	2,7	291	109	0.036
Norcarfentanil-2 (NCF2)	2,7	329	192	0.066
Carfentanil (CF1)	2	333	100	0.045
4-MeO-Bu Fentanyl	4	333	190	0.088
3Me Fentanyl	1	274	104	0.045
α-AcMe Fentanyl	6	274	142	0.058

Correlation Between Antigen Density and Peak Titer

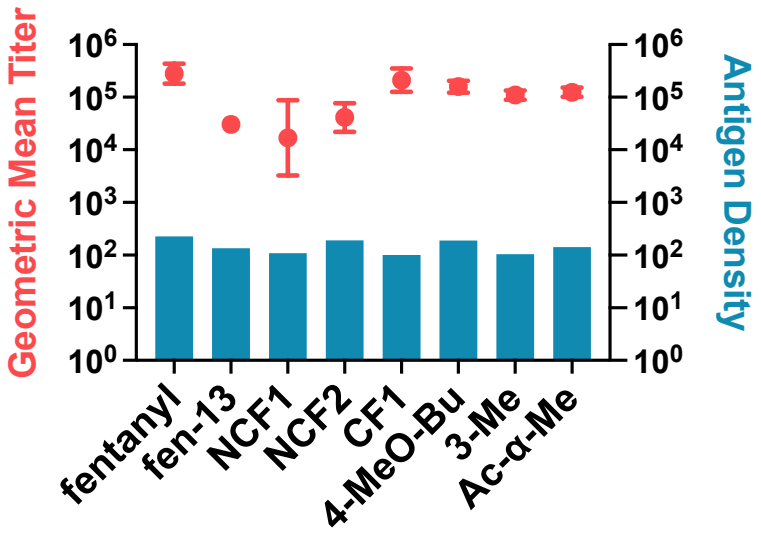

Cross Reactivity Data for All Clones

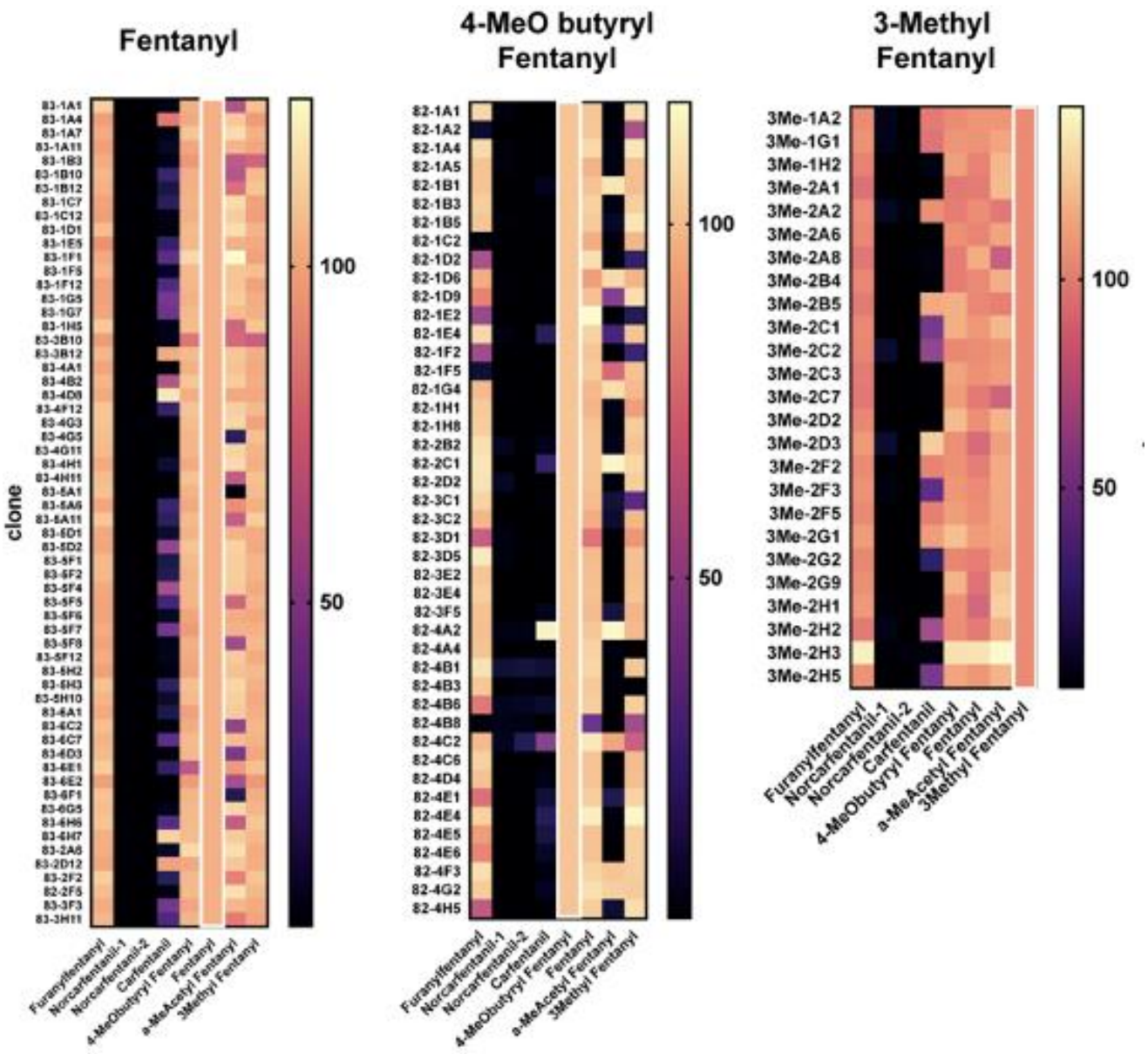

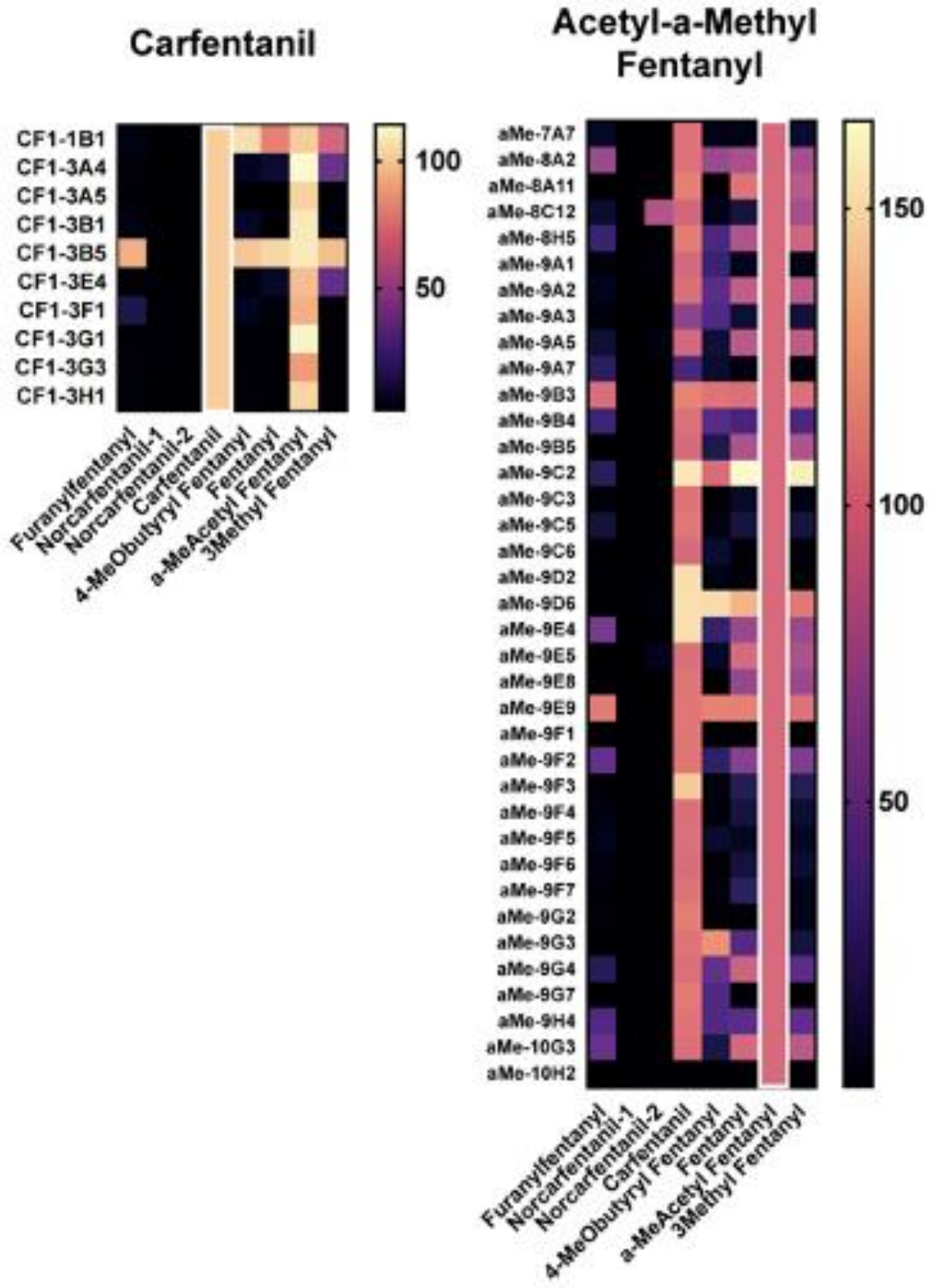
Carfentanil
CF1-1B1
CF1-3A4
CF1-3A5
CF1-3B1
CF1-3B5
CF1-3E4
CF1-3F1
CF1-3G1
CF1-3G3
CF1-3H1
100
50
Furanylfentanyl
Norcarfentanil-1
Norcarfentanil-2
Carfentanil
4-MeObutyryl Fentanyl
Fentanyl
a-MeAcetyl Fentanyl
3Methyl Fentanyl
Acetyl-a-Methyl Fentanyl
aMe-7A7
aMe-8A2
aMe-8A11
aMe-8C12
aMe-8H5
aMe-9A1
aMe-9A2
aMe-9A3
aMe-9A5
aMe-9A7
aMe-9B3
aMe-9B4
aMe-9B5
aMe-9C2
aMe-9C3
aMe-9C5
aMe-9C6
aMe-9D2
aMe-9D6
aMe-9E4
aMe-9E5
aMe-9E8
aMe-9E9
aMe-9F1
aMe-9F2
aMe-9F3
aMe-9F4
aMe-9F5
aMe-9F6
aMe-9F7
aMe-9G2
aMe-9G3
aMe-9G4
aMe-9G7
aMe-9H4
aMe-10G3
aMe-10H2
150
100
50
Furanylfentanyl
Norcarfentanil-1
Norcarfentanil-2
Carfentanil
4-MeObutyryl Fentanyl
Fentanyl
a-MeAcetyl Fentanyl
3Methyl Fentanyl

APPENDIX B: SARS-CoV-2 peptide conjugate vaccines

Characterization of genetically expressed PP7-Peptides

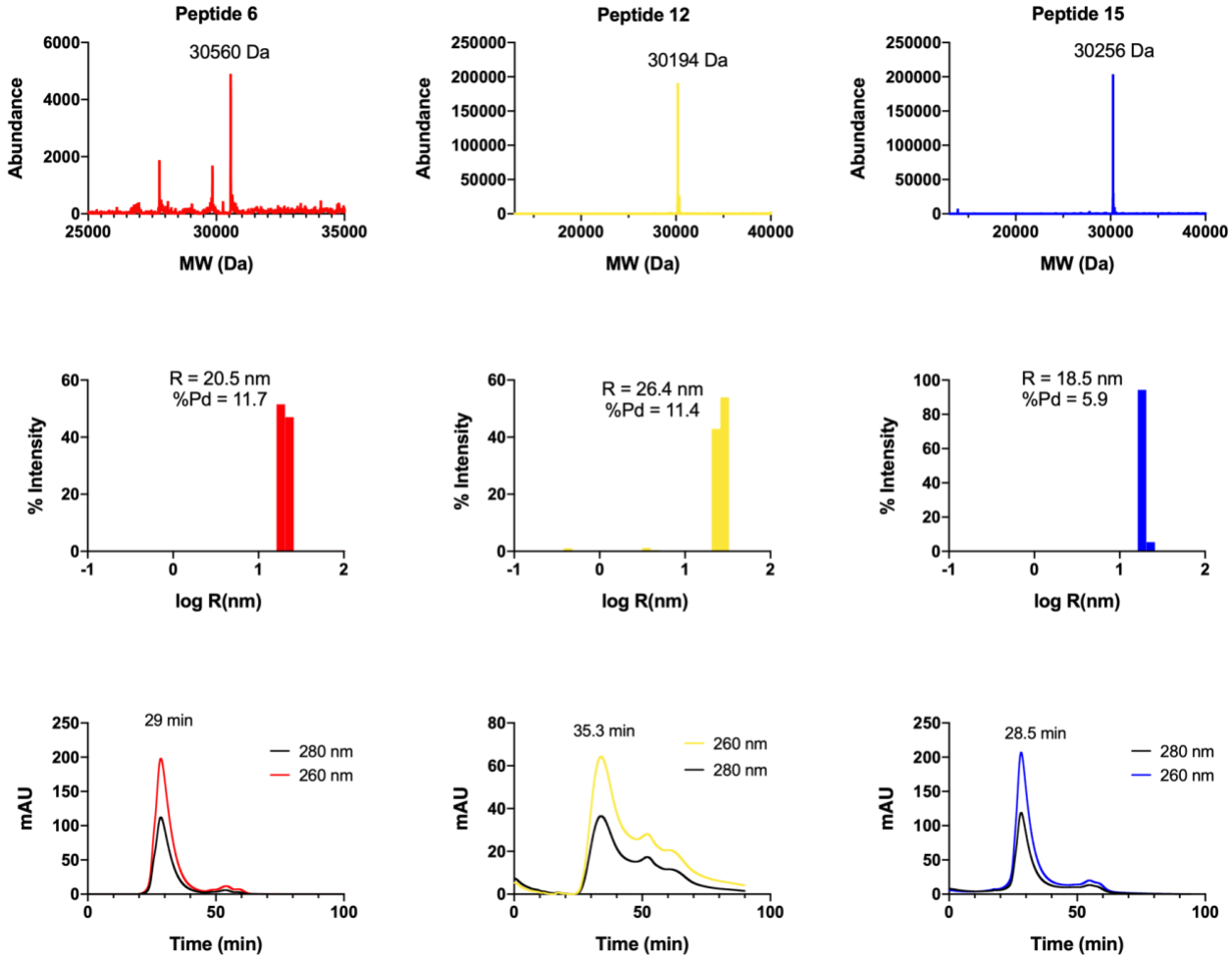

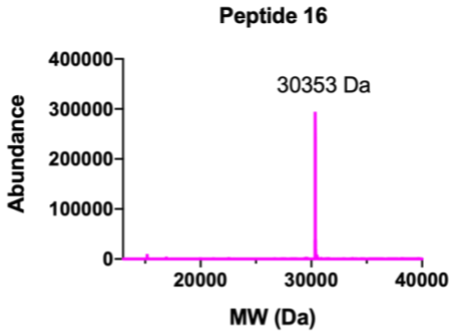
Peptide 16
30353 Da
Abundance
MW (Da)

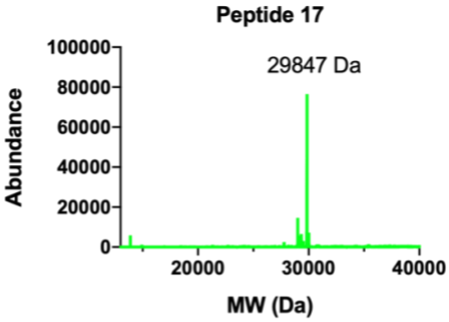
Peptide 17
29847 Da
Abundance
MW (Da)

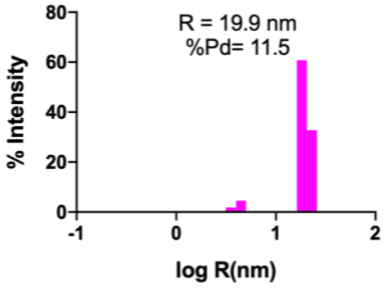
R = 19.9 nm
%Pd= 11.5
% Intensity
log R(nm)

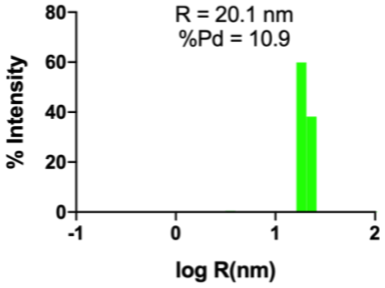
R = 20.1 nm
%Pd = 10.9
% Intensity
log R(nm)

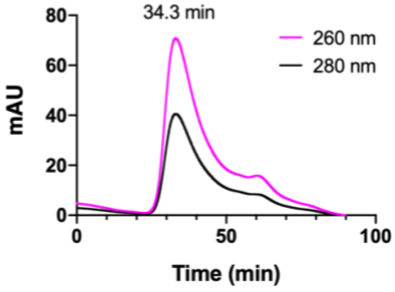
34.3 min
260 nm
280 nm
mAU
Time (min)

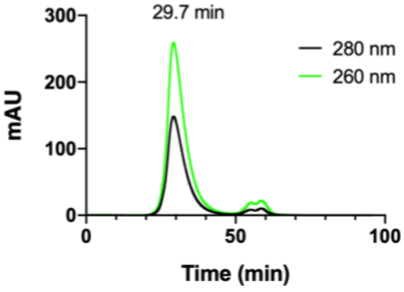
29.7 min
280 nm
260 nm
mAU
Time (min)

Characterization of chemically ligated VLP-Peptides

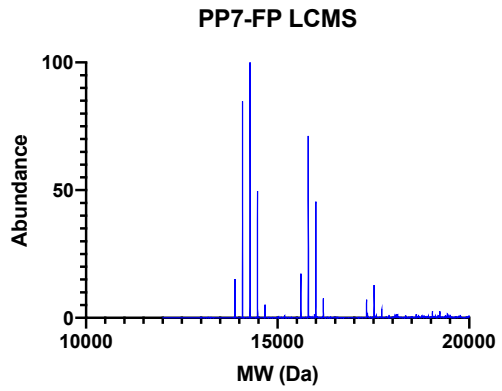

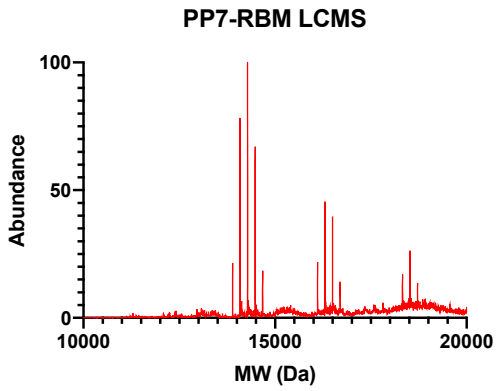

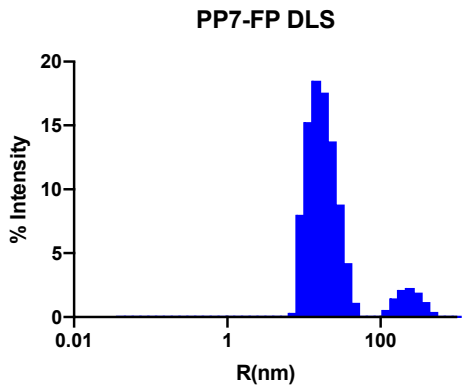

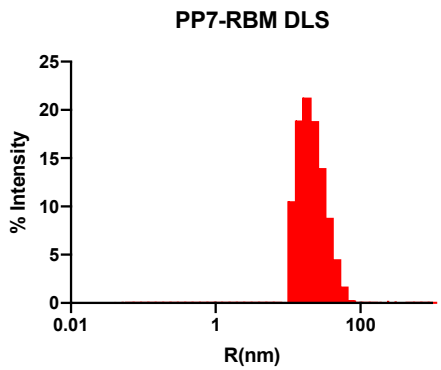

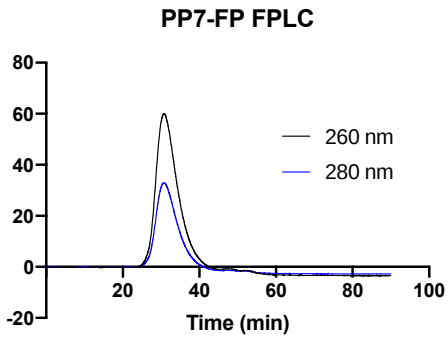

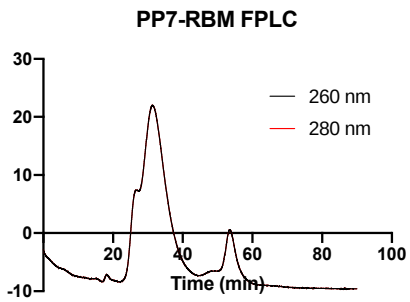

Binding Preference of Mutant Peptide Derived Clones to Ecto, RBD and Peptide

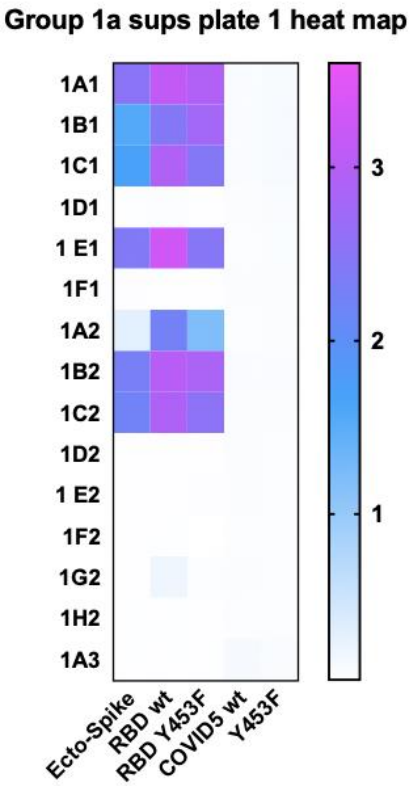

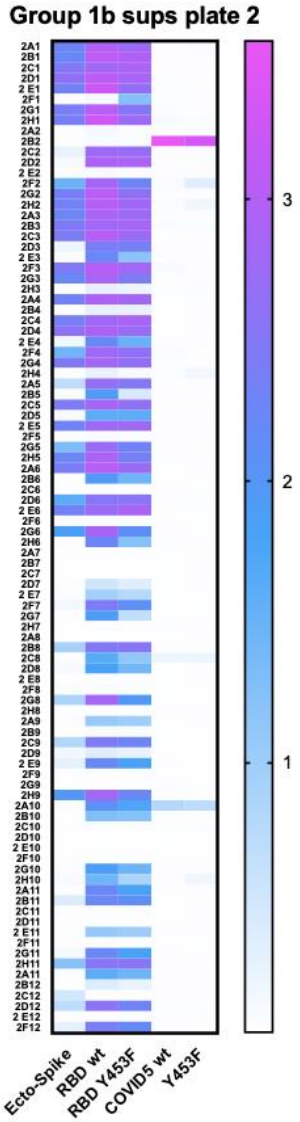

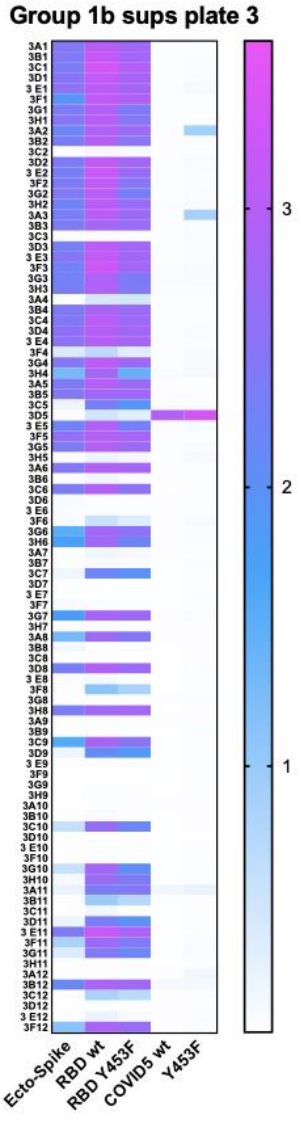

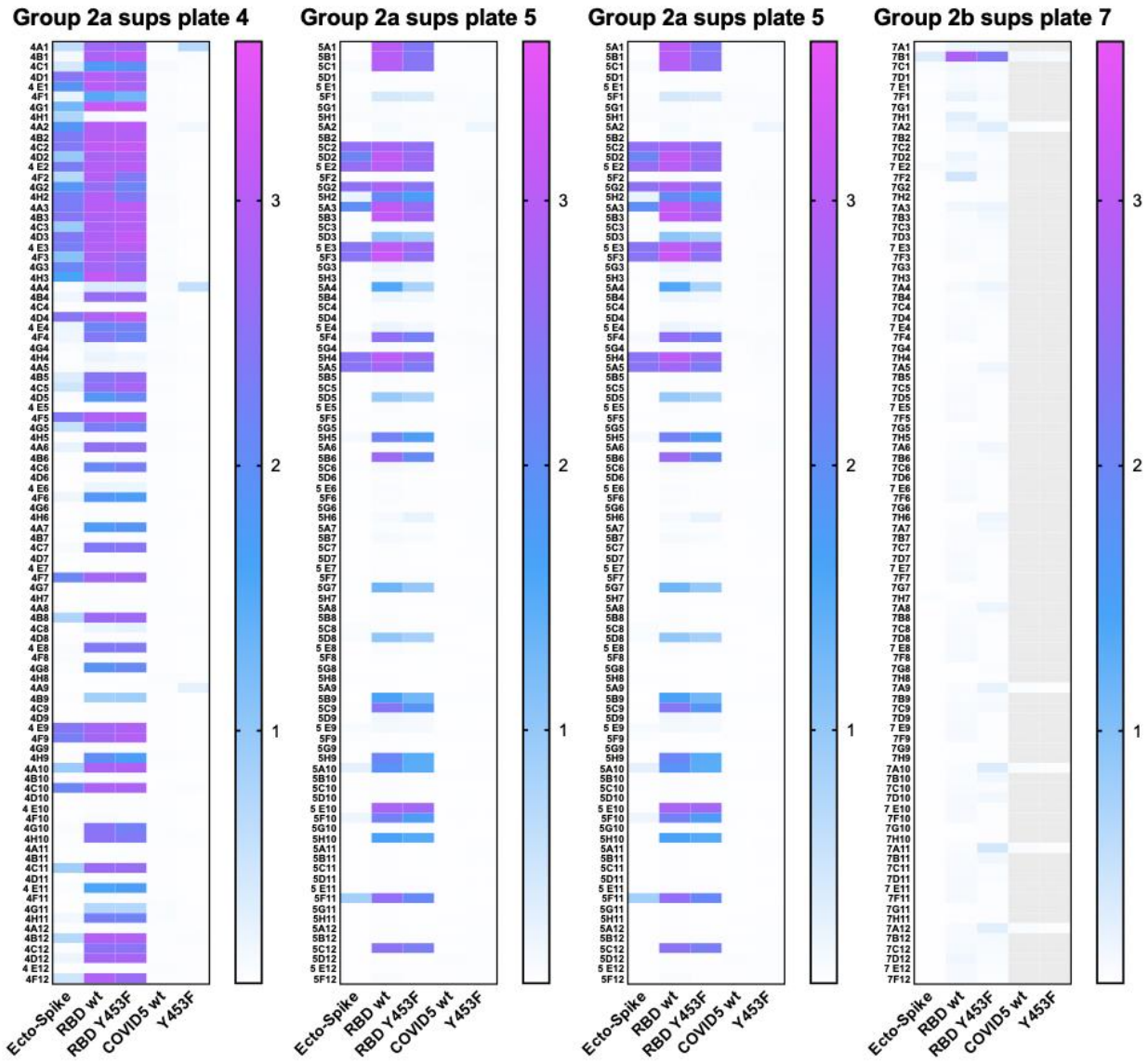
Group 2a sups plate 4
Group 2a sups plate 5
Group 2a sups plate 5
Group 2b sups plate 7
Ecto-Spike
RBD wt
RBD Y453F
COVID5 wt
Y453F
3
2
1